Role of pathogen-laden expiratory droplet dispersion and natural ventilation explaining a COVID-19 outbreak in a coach bus

To be submitted to Building and Environment 2022

Role of pathogen-laden expiratory droplet dispersion and natural ventilation explaining a COVID-19 outbreak in a coach bus

Qiqi Luo[a,b,#], Cuiyun Ou[a,b,#], Jian Hang[a,b*] , Zhiwen Luo[c], Hongyu Yang[a,b], Xia Yang[a,b], Xuelin Zhang[a,b], Yuguo Li[d], Xiaodan Fan[a,b]

[a] School of Atmospheric Sciences, Sun Yat-sen University, and Southern Marine Science and Engineering Guangdong Laboratory (Zhuhai), Zhuhai, China

[b] Key Laboratory of Tropical Atmosphere-Ocean System (Sun Yat-sen University), Ministry of Education, Zhuhai (519000), China

[c] School of the Built Environment, University of Reading, Reading, UK

[d] Department of Mechanical Engineering, The University of Hong Kong, Hong Kong SAR, China

[#] First authors: Qiqi Luo, Cuiyun Ou

[*]Corresponding author: Jian Hang

School of Atmospheric Sciences, Sun Yat-sen University, Zhuhai, China

Tel: +86-13710248541

E-mail address: hangj3@mail.sysu.edu.cn

Abbreviations

ACH	Air change rates per hour [h^{-1}]	N	Total released droplet number
ASHRAE	American Society of Heating, Refrigerating and Air-Conditioning Engineers	n	Number of droplets
		NMSE	Normalized mean square error
		N_i	Passenger inhaled droplet number
		N_S	Passenger inhaled pathogen-laden droplet number
C	Particle concentration [μg/m^3]		
C_2H_6	Ethane	p	Pulmonary ventilation rate [m^3/s]
C_c	Cunningham slip correction	P	Infection risk
CCTV	Closed-circuit television	PLD	Pathogen-laden droplets
C_d	Quantum concentration of droplets [quanta/m^3]	p_s	Pulmonary ventilation rate of index patient [m^3/s]
C_e	Particle concentration at exhaust [μg/m^3]	q	Quanta generation rate [quanta/s]
		Q	Ventilation rate [m^3/s]
CFD	Computational fluid dynamics	Re_p	Reynolds number
C_g	Tracer gas concentration	RH	Ambient relative humidity
$C_{g,p}$	Tracer gas concentration at passenger's nose [ppm]	RNG	Renormalization group
		SARS-CoV-2	Severe acute respiratory syndrome coronavirus 2
$C_{g,q}$	Quantum concentration of tracer gas [quanta/m^3]	$S_{susceptible}$	Number of susceptible people
$C_{g,s}$	Tracer gas concentration at patient [ppm]	t	Time [s]
		T	Temperature [K]
$C_{i,s}$	Vapor concentration at droplet surface [kg·mol·m^{-3}]	t_0	Exposure period [s]
		T_e	Temperature at exhaust [K]
$C_{i,sr}$	Vapor concentration of bulk [kg·mol·m^{-3}]	TIF	30-minute-exposure intake fraction
		TIR	30-minute-exposure infection risk
$C_{infected}$	Number of infected cases	T_s	Temperature at inlet [K]
COVID-19	Corona virus disease 2019	U	Normalized velocity
C_s	Particle concentration at inlet [μg/m^3]	$u_{p,i}$	Droplet velocity (m/s)
		u_s	Supply air velocity [m/s]
C_v	Virus concentration	V	Velocity [m/s]
D	Dilution ratio	V_{Bus}	Speed of bus [m/s]
d_p	Initial droplet diameter [μm]	Vol	Volume [m^3]
$F_{a,i}$	Additional forces [N]	W	Width [m]
FB	Fractional bias	WHO	World Health Organization
f_D	Stoke's drag modification	WIR	Whole-journal-exposure infection
$F_{drag,i}$	Drag force [N]	$x_{p,i}$	Droplet displacement [m]
$F_{g,i}$	Gravitational force [N]	Z	Poles height [m]
g	Gravitational acceleration	μ_t	Turbulent viscosity [kg·m^{-1}·s^{-1}]
H	Height [m]	ε	Normalized particle concentration
HVAC	Heating, Ventilation and Air Conditioning	θ	Normalized temperature
		λ	Molecular mean free path of air [m]
I	Number of infectors	ρ	Density of air [kg/m^3]
k_c	Mass transfer coefficient [m/s]	ρ_p	Density of droplets [kg/m^3]
L	Length [m]	τ_p	Aerosol characteristic response

Abstract

The influencing mechanism of droplet transmissions inside crowded and poorly ventilated buses on infection risks of respiratory diseases is still unclear. Based on experiments of one-infecting-seven COVID-19 outbreak with an index patient at bus rear, we conducted CFD simulations to investigate integrated effects of initial droplet diameters(tracer gas, 5μm, 50μm and 100μm), natural air change rates per hour(ACH=0.62, 2.27 and 5.66h^{-1} related to bus speeds) and relative humidity(RH=35% and 95%) on pathogen-laden droplet dispersion and infection risks. Outdoor pressure difference around bus surfaces introduces natural ventilation airflow entering from bus-rear skylight and leaving from the front one. When ACH=0.62h^{-1}(idling state), the 30-minute-exposure infection risk(TIR) of tracer gas is 15.3%(bus rear) - 11.1%(bus front), and decreases to 3.1%(bus rear)-1.3%(bus front) under ACH=5.66h^{-1}(high bus speed).The TIR of large droplets(i.e., 100μm/50μm) is almost independent of ACH, with a peak value(~3.1%) near the index patient, because over 99.5%/97.0% of droplets deposit locally due to gravity. Moreover, 5μm droplets can disperse further with the increasing ventilation. However, TIR for 5μm droplets at ACH=5.66h^{-1} stays relatively small for rear passengers(maximum 0.4%), and is even smaller in the bus middle and front(<0.1%). This study verifies that differing from general rooms, most 5μm droplets deposit on the route through the long-and-narrow bus space with large-area surfaces(L~11.4m). Therefore, tracer gas can only simulate fine droplet with little deposition but cannot replace 5-100μm droplet dispersion in coach buses.

Keywords: Computational fluid dynamics **(**CFD) simulation, droplet dispersion, infection risk (*IR*), natural air change rate (*ACH*), aerosol inhalation transmission, COVID-19

1. Introduction

Respiratory infectious diseases, such as influenza, severe acute respiratory syndrome (SARS) and coronavirus disease 2019 (COVID-19), have threatened public health in the last two decades [1]. In particular, the recent COVID-19 pandemic is caused by severe acute respiratory syndrome coronavirus 2 (SARS-CoV-2). By 27 January 2022, more than 352 million people had been diagnosed with COVID-19, of whom more than 3.5 million had died[2]. Most of the human-to-human infections may occur in various indoor environments via droplet transmissions.

Numerous studies have demonstrated that respiratory infections may occur through the transmission of virus-laden droplets or droplet nuclei [3-5]. Pathogen-laden droplets (PLD) exhaled from the infected people may be the medium of human-to-human infection, because the pathogens can survive in the air for a period of time. Taking the current prevalence of COVID-19 for instance, the half-life of SARS-CoV-2 virus in the air is reported to be on the order of magnitude of one hour [6]. Recent studies have redefined that there are three main transmission routes of respiratory infection: surface touch transmission, drop spray transmission and aerosol inhalation transmission [7, 8]. Among them, aerosol inhalation transmission happens when air-suspended PLD are inhaled by a susceptible person. Ventilation modes and hourly air change rates (*ACH*) have been verified as the key factors affecting aerosol inhalation transmission and indoor infection risks [9-11].

There have been numerous studies on indoor ventilation, droplet/tracer gas dispersion and exposure analysis in inter-unit residential buildings [12-16], general indoor environments with mixing or displacement ventilation [17-19], and specific indoor space, for instance, restaurants [10, 20] and hospital wards [21, 22]. Particularly,

74 for the indoor environment of public transportation, most previous researches focused
75 on airplane cabins [23-25] and high-speed trains [26, 27].

76 Although the coach bus is one of the most popular transportation modes for inter-
77 city and suburban transportation, investigations on their indoor environments and
78 infection risk are limited so far [28, 29]. Due to the unopenable windows, the crowded
79 coach bus often obtains fresh air from the skylight suppliers which is related to the
80 running conditions. When the HVAC (Heating, Ventilation and Air Conditioning) is on,
81 there is only indoor circulation, resulting in an insufficiently ventilated indoor
82 environment. Therefore, the coach bus is conducive to the transmission of respiratory
83 infectious diseases, which is worthy of study.

84 Our previous researches [11] reported that there was a COVID-19 outbreak with 7
85 non-associated infected passengers on a coach bus with insufficient natural ventilation
86 in January 2020 (winter) in Hunan Province, China. In this study, we first conducted
87 field experiments, and then numerically simulated the tracer gas dispersion under the
88 measured mean ventilation condition [11]. However, since the coach bus was driving
89 in three states (high bus speed, low bus speed and idling), corresponding to different
90 natural ventilation rates, a further detailed case study is required to investigate the
91 influence of different natural ventilation rates on droplet dispersion and resulting
92 infection risk. In addition, the initial diameter of exhaled droplets is in a large range
93 (0.1-100 μm) [30, 31]. Moreover, numerous studies [18, 32, 33] have indicated that the
94 droplet evaporation correlated to initial droplet diameters and *RH* significantly
95 influence their gravity force and deposition effects, which integrates with turbulent
96 diffusion, drag force, Saffman's lift force, and so on. Such complicated processes

should be considered for more comprehensive investigations on transmission mechanisms and assessments of human-to-human exposure and infection risk.

Many studies have confirmed that the transport behavior of droplets smaller than 5 μm is similar to that of tracer gas in a room [34-37]. However, the indoor environment of the bus is different from that of ordinary rooms, because the bus is long and narrow with more obstacles and more complex indoor airflow. In addition, *RH* is considered to influence droplet dispersion in indoor environments[17, 32, 38]. Therefore, two questions need to be answered: does tracer gas still have a similar transmission with droplets smaller than 5 μm in the bus environment? does *RH* still obviously affect droplet dispersion in the buses? For the bus environments, the feasibility of adopting tracer gas to replace fine droplets and the effect of *RH* on droplet dispersion need further exploration.

In the present study, by performing computational fluid dynamics (CFD) simulations, we further investigate the integrated impacts of *RH* (35%, 95%), initial droplet diameters (tracer gas, 5 μm, 50 μm, 100 μm), natural ventilation rates (*ACH* = 0.62 h^{-1}, 2.27 h^{-1}, 5.66 h^{-1} respectively related to idling, low bus speed, and high bus speed), and body thermal plumes on the evaporation and dispersion of exhaled droplets in this enclosed coach bus. We also predict the difference of exposure/infection risk for various pathogen-laden expiratory droplets under different conditions.

2. Methodology

2.1. Full-scale experimental bus

Fig. 1 shows the detailed model descriptions of the target coach bus with a cabin size of 11.4 m × 2.5 m × 2 m ($L \times W \times H$), where occcured a COVID-19 epidemic during the 200-minute long-route journey on January 22, 2020 [11]. It was a double-deck 47-seat bus with the passenger cabin on the upper deck and the driver zone on the lower deck. Only the radiator at the index-patient side was functional and turned on during the whole journey, the other side was broken. As shown in Fig. 1b, the cabin was fully occupied except Seat 8C (46 passengers in total). An index patient (in scarlet) at seat 12D returned home from Changsha city, Hunan province, China, eventually infecting seven of the passengers. These infected passengers (in pink) were respectively located at seats 1D, 5C, 6A, 6D, 9C, 9D and 13D. Among them, the passenger at seat 1D is farthest away from the index patient, at a distance of 9.46 m.

All the windows could not be opened with the skylights (as shown in Fig. 1a) for natural ventilation. Fresh air entered the bus through the skylight inlet at the rear ceiling, and contaminated air escaped from the skylight outlet at the front ceiling (Fig. 1a). The measured *ACH* could change with the various air pressure difference between the indoor and outdoor of the bus due to the various running speeds. More detailed information about the experimental setup can be found in our previous study [11].

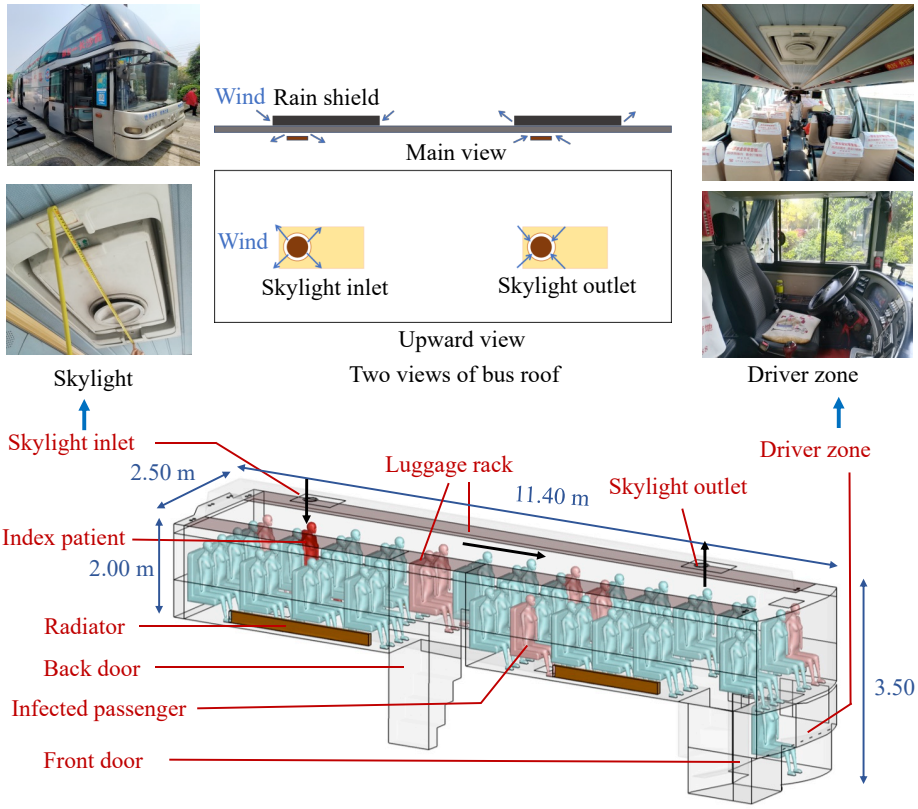
Wind
Rain shield
Main view
Wind
Skylight inlet
Skylight outlet
Upward view
Two views of bus roof
Skylight
Driver zone
Skylight inlet
2.50 m
Luggage rack
11.40 m
Skylight outlet
Driver zone
Index patient
2.00 m
Radiator
Back door
Infected passenger
Front door
3.50 m

(a)

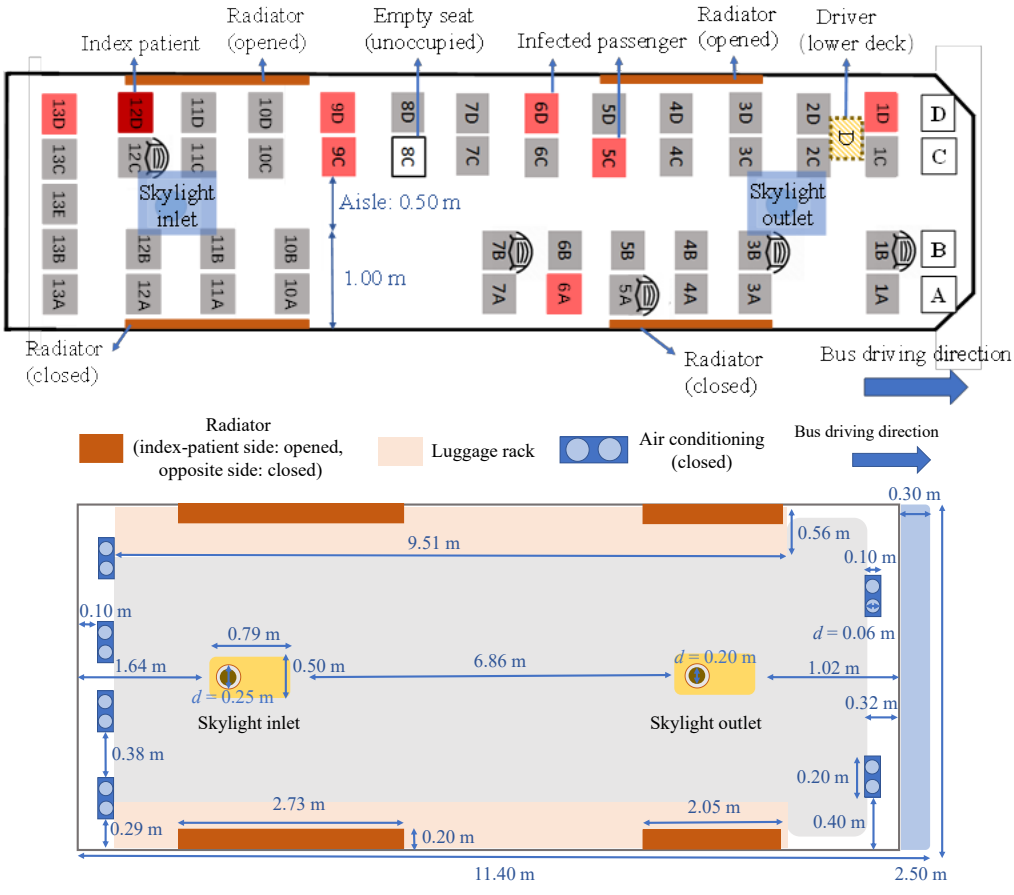
Index patient
Radiator (opened)
Empty seat (unoccupied)
Infected passenger
Radiator (opened)
Driver (lower deck)
Skylight inlet
Aisle: 0.50 m
1.00 m
Skylight outlet
Radiator (closed)
Radiator (closed)
Bus driving direction
Radiator (index-patient side: opened, opposite side: closed)
Luggage rack
Air conditioning (closed)
Bus driving direction
0.30 m
9.51 m
0.56 m
0.10 m
0.10 m
0.79 m
d = 0.06 m
1.64 m
0.50 m
6.86 m
d = 0.20 m
1.02 m
d = 0.25 m
Skylight inlet
Skylight outlet
0.32 m
0.38 m
0.20 m
2.73 m
2.05 m
0.29 m
0.20 m
0.40 m
11.40 m
2.50 m

(b)

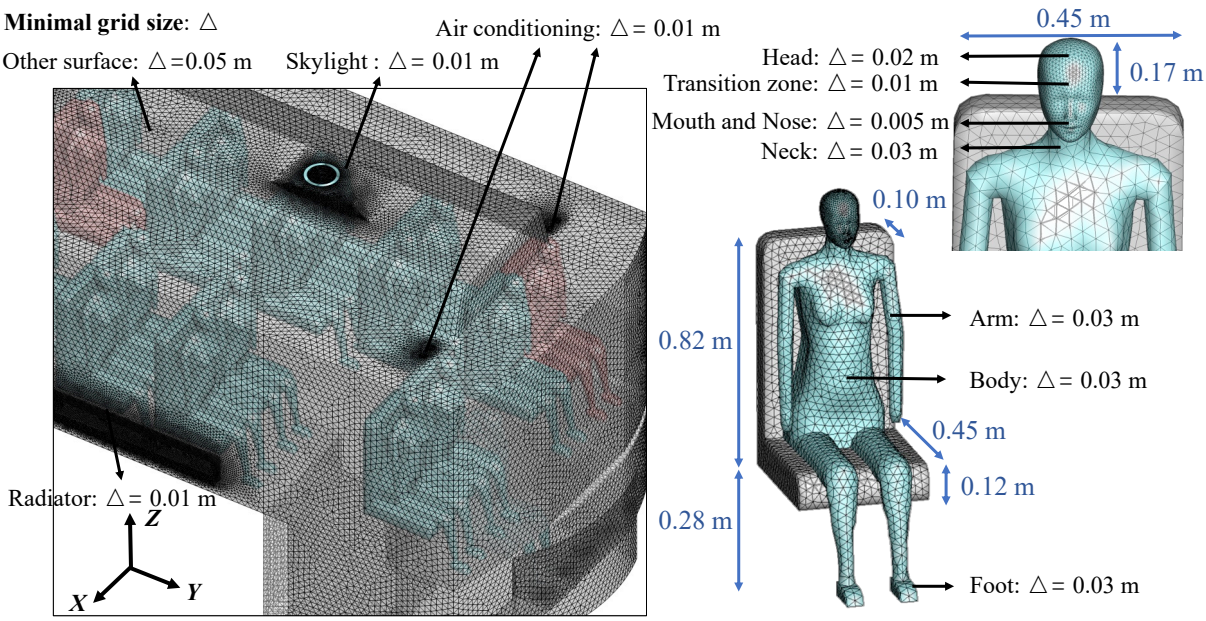

(c)

Fig. 1. (a) Bus photos and 3D bus model, (b) Bus top view and size information, (c) Grid arrangements of model.

137

138 ***2.2. Numerical modeling of bus ventilation and droplet dispersion***

139 ***2.2.1. Descriptions of bus model and case studies***

140 We utilized Gambit to build the bus cabin and manikin models (Fig. 1). We created
141 a refined grid with 0.005 m size on mouth and nose, which is smaller than the grid of
142 0.03 m size around the human body, 0.01 m mesh size on the skylight inlet/outlet and
143 heat radiator, and 0.05 m for the bus body (Fig. 1c). A total number of 5,379,993
144 unstructured meshes were generated, which was verified to ensure grid-independent
145 requirements.

146 Twenty-one cases were considered as shown in Table 1. We investigated the
147 influence of *ACH* (0.62, 2.27 and 5.66 h^{-1}) related to bus speed (0, 30 and 80-90 km/h),
148 initial droplet diameters (tracer gas, d_p = 5, 50 and 100 μm), and ambient relative
149 humidity (*RH* = 35%, 95%) on the transmission of the index patient's exhaled droplets

and the exposure/infection risk of other passengers. Ethane (C_2H_6) was adopted as the tracer gas to explore the dispersion difference between droplets and tracer gas in the coach bus.

Table 1
Parameters and setups in all 21 test cases.

Experimental variables	Setup	Notes
Ventilation rate (ACH / h^{-1})	0.62 h^{-1}	Bus is at idling (V_{Bus} = 0 km/h).
	2.27 h^{-1}	Bus is running at low speed (V_{Bus} = 30 km/h).
	5.66 h^{-1}	Bus is running at high speed (V_{Bus} = 80-90 km/h).
Initial droplet diameter (d_p / μm)	Tracer gas	As a surrogate for fine droplets and droplet nuclei.
	5 μm	For effect of initial diameter on droplet dispersion.
	50 μm	
	100 μm	
Ambient relative humidity (RH / %)	35%	For effect of RH on droplet dispersion.
	95%	

2.2.2. Numerical simulation of airflow model

The renormalization group (RNG) k-ε model [39] has been verified to effectively simulate indoor airflows and tracer gas dispersion with considerable accuracy and computing efficiency [40-42]. Thus, we adopted Ansys FLUENT with RNG k-ε model to solve the conservation equations for mass, momentum, energy, humidity and turbulence variables. All the governing equations were discretized by the finite volume method in the second-order upwind scheme. SIMPLE scheme was selected to couple the pressure and velocity. Boussinesq hypothesis was adopted to consider the influence of thermal buoyancy.

To simulate the airflow field, we assumed that the variables were unchanging (steady) in the bus. CFD simulations were run until residuals became constant, for all

cases the iterations were over 100,000 times. Convergence was achieved after non-dimensional residuals for continuity equation, velocity components, energy, k and ε were below 10^{-3}, 10^{-4}, 10^{-6}, 10^{-4} and 10^{-4}, respectively and the monitored variables at specific surfaces were stable. We also checked energy balance and mass balance to help determine the convergence.

2.2.3. Droplet dispersion modeling

After the steady airflow field calculation was solved, we started the simulation of tracer gas dispersion and particle tracking, separately. The second-order upwind scheme was adopted in the tracer gas simulation. The mass fraction of C_2H_6 in the index patient's exhalation flows was 0.32 in CFD simulations according to Ou et al. [11]. Lagrangian method with the Discrete Phase Modeling (DPM) was adopted to simulate the droplet dispersion with initial diameters of 5 μm, 50 μm and 100 μm [28, 43]. Lagrangian equations of the droplets for i direction are as follows:

$$\frac{dx_{p,i}}{dt} = u_{p,i} \tag{1}$$

$$\frac{du_{p,i}}{dt} = \sum F_i = F_{drag,i} + F_{g,i} + F_{a,i} \tag{2}$$

$$F_{drag,i} = \frac{f_D}{\tau_p}(u_i - u_{p,i}) \tag{3}$$

$$F_{g,i} = \frac{g_i}{\rho_p}(\rho_p - \rho) \tag{4}$$

where $x_{p,i}$ *and* $u_{p,i}$ are the droplet displacement (m) and velocity (m/s) in i direction, respectively; $F_{drag,i}$ is the drag force (Eq. (3)), $F_{g,i}$ is the gravitational force (Eq. (4)). In addition, $F_{a,i}$ is the additional forces (Eq. (2)) for which we only considered Brownian force and Saffman's lift force [28, 44]. ρ_p and ρ are the density of droplets and air,

187 respectively. f_D is the Stoke's drag modification function of Reynolds number for large
188 aerosol (Re_p) [45].

189 $$f_D(Re_p) = 1+0.15Re_p^{0.687} \quad (5)$$

190 In Eq. (3), τ_p is the aerosol characteristic response time, which is defined as:

191 $$\tau_p = \frac{\rho_p d_p^2 C_c}{18\mu_t} \quad (6)$$

192 where μ_t is the turbulent viscosity (kg $m^{-1}\cdot s^{-1}$) and d_p is the droplet diameter. C_c is
193 the Cunningham slip correction factor, which is defined as [46]:

194 $$C_c = 1+ \frac{2\lambda}{d_p}[1.257+0.4\ \exp(-\frac{1.1d_p}{2\lambda})] \quad (7)$$

195 where λ is the molecular mean free path of air.

196 In CFD simulations, the mass ratio of liquid (water) and solid element (sodium
197 chloride) in droplets is assumed as 9 [47]. The densities of water liquid and sodium
198 chloride are respectively 998.2 kg/m^3 and 2170 kg/m^3. The evaporation process will
199 continue until the droplets' volatile composition (i.e., water) is completely consumed.
200 The vaporization rate is governed by the gradient of the vapor concentrations between
201 the droplet surface and the bulk gas. The molar flux of vapor is defined as:

202 $$N_i = k_c\ (C_{i,s}-C_{i,sr}) \quad (8)$$

203 where k_c is the mass transfer coefficient (m/s) which can be obtained by Sherwood
204 relationship [48]. The vapor concentrations at both droplet surface $C_{i,s}$ (kg·mol·m^{-3})
205 and bulk air $C_{i,sr}$ (kg·mol·m^{-3}) are calculated by the assumption of the ideal gas.

206 ***2.2.4. Boundary conditions***

Table 2
Boundary condition setups in CFD simulation.

Boundary name	Boundary condition
Skylight inlet	**Velocity inlet**, velocity is different with various running conditions (idling: 0.57 m/s, low bus speed: 2.09 m/s, high bus speed: 5.37 m/s), temperature is 11 ℃, turbulent intensity is 5 %.
Skylight outlet	**Outflow**, velocity is same as skylight inlet, temperature is different with various running conditions (idling: 24 ℃, low bus speed: 23 ℃, high bus speed: 21 ℃), turbulent intensity is 5 %.
Glass at wall surface	**No slip wall**, heat flux is determined by energy balance estimates (idling: 92.89 W/m^2, low bus speed: 79.00 W/m^2, high bus speed: 56.63 W/m^2).
Index-patient side radiator	**Standard wall function, no slip wall**, heat flux is 100 W/m^2, surface area is 3.38 m^2.
Opposite side radiator (closed)	**Standard wall function, no slip wall**, heat flux is 0 W/m^2, surface area is 3.38 m^2.
Wall of bus, luggage rack, seat	**Standard wall function, no slip wall**, heat flux is 0 W/m^2.
Nose (except index patient)	**Mass-flow-outlet**, mass flow rate is 9.23×10^{-5} kg/s, Nostril area is 2.87×10^{-4} m^2.
Mouth of index patient	**Velocity inlet,** exhaled airflow velocity is 1.5 m/s (in a direction paralleling to Y-axis), temperature is 32 ℃.
Other body surface	**Standard wall function, no slip wall**, convective heat is 50 W for each person.

207

208 Table 2 shows the relevant boundary condition settings in CFD simulations [11].
209 At the skylight inlet, the ambient air temperature was set as 11 ℃, and the inlet velocity
210 was set as 0.57, 2.09 and 5.37 m/s according to the measured *ACH*. At the skylight
211 outlet, the air temperature was set as 24, 23, 21 ℃ according to the experiment. Non-
212 slip wall with standard wall function was applied at all wall surfaces. The effects of
213 human respiration and body surface heat fluxes were considered, with convective heat
214 fluxes of 50 W for each sedentary passenger. To simplify the calculations, it was
215 assumed that the droplets were exhaled from the mouth of the index patient, while the

other passengers only inhaled through noses. A value of heat flux determined by the energy balance estimates was set on the bus window glasses [11].

After the steady airflow field with water vapor was solved, the single-diameter droplets were uniformly released from the mouth of the index patient at a rate of 20 droplets per time step ($t = 0.1$s, 18,000 iterations in total). The initial velocity of exhaled droplets was 1.5 m/s and the initial temperature was 32 ℃. After 30 min continuous releasing, we got a fully-developed droplet distribution with a total droplet number of 360, 000. When a droplet encountered a surface, it would have three different fates: trap, reflect and escape. As shown in Table 3, different droplet sizes, surface roughness and other factors would lead to different boundary conditions of droplets on the surfaces [28, 49]. The trap condition was utilized for the floor, human surfaces and seats, which means droplets were trapped once they touched the objects and the trajectory calculations were terminated. While for the glass, roof, luggage racks and vertical walls, the reflect condition was applied due to smooth surfaces or gravity, which means droplets rebound off the surface and continue dispersion [28, 44, 50]. Escape condition was adopted to the skylight outlet and passengers' noses (except the index patient). Some of the CFD simulations in this study were completed on the Tianhe II supercomputer with the support of the National Supercomputer Center in Guangzhou.

Table 3

Boundary conditions of each boundary in Discrete Phase Model.

Boundary name	Boundary conditions
Skylight, nose of passenger (except index patient)	Escape (trajectory calculations terminated)
Glass at wall surface, roof, luggage rack, vertical wall	Reflect (droplets suspended in air)
Floor, air conditioning, radiator, human body surface, seat	Trap (trajectory calculations terminated)

2.3. Calculation of infection risk

We adopted the Wells-Riley equation to calculate each passenger's infection risk of aerosol inhalation transmission, which represented the probability of infection through inhaling PLD. This method has been verified to effectively predict the infection risk [51-53]. The Wells-Riley equation is defined as follows [54]:

$$P = \frac{C_{infected}}{S_{susceptible}} = 1\text{-}e^{-\frac{Iqpt}{Q}} = 1\text{-}e^{-N_S} \tag{9}$$

where P is the probability of infection risk; $C_{infected}$ is the number of infected cases; $S_{susceptible}$ is the number of susceptible people; I is the number of people in the infectious stage or infectors; q is the quanta of PLD produced per infector per second (quanta/s); p is the pulmonary ventilation rate of each susceptible (m^3/s); Q is the room ventilation rate with virus-free air (m^3/s); t is the exposure time (s); N_S is the number of PLD inhaled by susceptible person, which was calculated for droplets and tracer gas by using different equations.

For droplets, N_S is defined as [54]:

$$N_s(x, t_0) = C_v p \int_0^{t_0} C_d(t)\mathrm{d}t = C_v N_i \tag{10}$$

where C_v is the concentration of the virus in the exhaled droplets; $C_d(t)$ is the quanta concentration in an indoor environment at the time t (quanta/m^3); t_0 is the exposure period; N_i is the total number of droplets (exhaled from the index patient) inhaled by passengers.

For tracer gas, N_S is defined as Eq. (11) according to the dilution-based evaluation method [55]:

$$N_s = \int_0^{t_0} p C_{g,q}(t)\mathrm{d}t \tag{11}$$

where $C_{g,q}$ is the airborne quanta concentration at the target position (quanta/m^3), and defined as $C_{g,q} = \frac{qC_{g,p}}{p_s C_{g,s}}$, where p_s is the breathing rate of the infector (m^3/s); $C_{g,s}$ and $C_{g,p}$ are the airborne contaminant concentrations (ppm) at the source and target position, respectively.

Despite a critical parameter for calculating the infection risk, the value of q from a COVID-19 infector is currently not officially established. In this realistic bus outbreak, there were one infector (I = 1) and 45 susceptible passengers ($S_{susceptible}$ = 45), seven of whom were infected ($C_{infected}$ = 7). According to the travel history, this bus drove for 145 min at high speed (Q = 5.69 m^3/min, t = 145 min), 45 min at low speed (Q = 2.28 m^3/min, t = 45 min) and 10 min at idling (Q = 0.62 m^3/min, t = 10 min). Substituting these data into Eq. (9) could back-calculate the value of q as 0.61 min^{-1} (36.6 h^{-1}). This value agrees well with the range of 14–48 h^{-1} obtained by Dai and Zhao [56] who adopted a reproductive number-based fitting approach.

Ansys FLUENT was employed to simulate the number of droplets inhaled by each passenger (N_i) and the concentration of tracer gas ($C_{g,s}$ and $C_{g,p}$). Then the N_S for droplets and tracer gas were respectively obtained by Eq. (10) and Eq. (11). Finally, the infection risk of each passenger was calculated by Eq. (9) for both droplets and tracer gas. In order to compare the infection risk under various ventilation rates, we carried out a 30-minute simulation for each vehicle driving situation.

2.4. Validation of numerical modeling

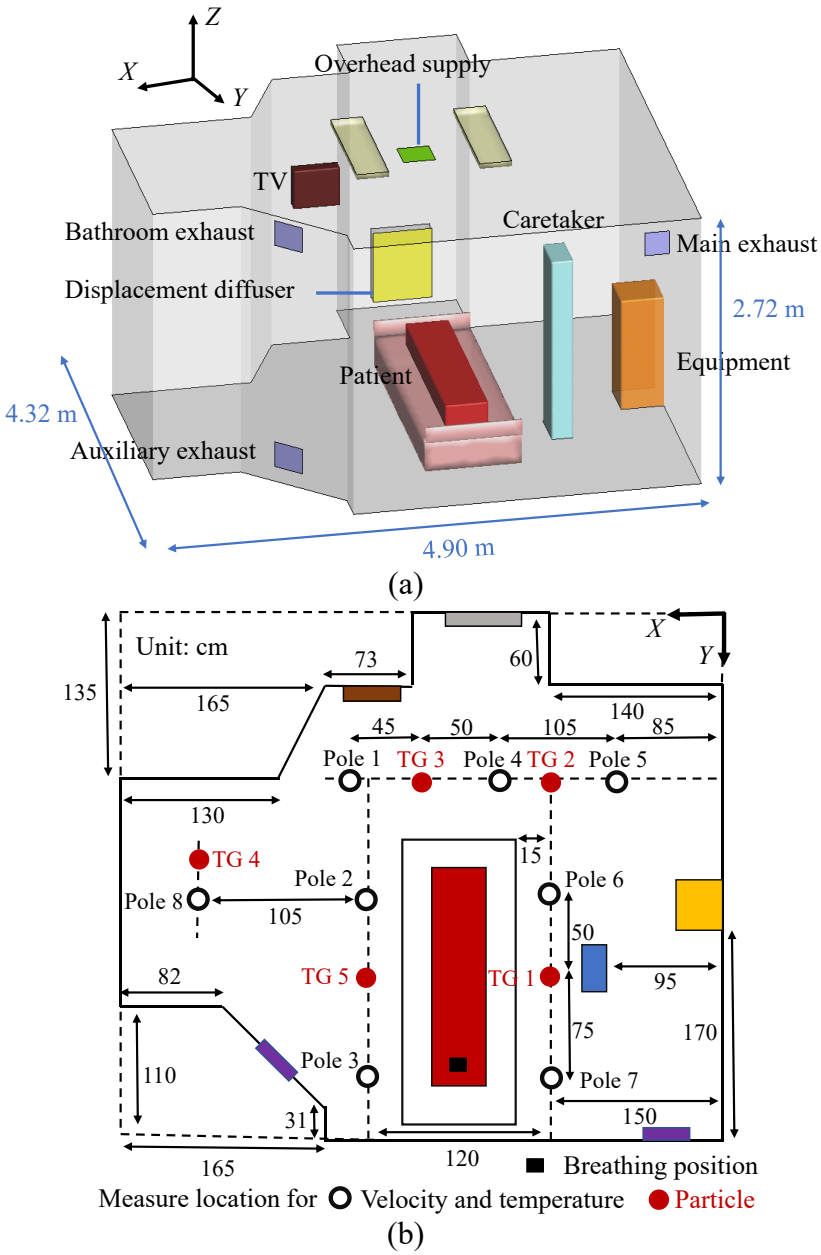

Fig. 2. Model setups of single-bed isolation room in CFD validation case (Yin et al., 2009).

279

280 Firstly, we performed a set of dispersion tests for validating the CFD predictions
281 of tracer gas dispersion. The evaluation of tracer gas dispersion by this field
282 experimental data can refer to our previous study [11].

283 In addition, we further carried out a validation study of indoor airflows,
284 temperature and tracer gas/particle dispersion in a hospital ward evaluated by the
285 experiment conducted by Yin et al. [36]. As shown in Fig. 2a, the experiment was
286 performed in a full-scale one-person patient ward (4.90 m × 4.32 m × 2.72 m). The
287 ventilation rate from the displacement diffuser was 0.054 m^3/s (4 ACH) and the
288 temperature was 19.5 °C. The ventilation rates of bathroom exhaust and main exhaust
289 were 0.017 m^3/s and 0.037 m^3/s , respectively. As shown in Fig. 2b, the air velocity and
290 temperature were measured at seven heights of Poles 1-8. Particle concentration was
291 measured at poles TG1 - TG5 at six heights. More details about the experimental setups
292 could be found in Yin et al. [36].

293 In this validation, we adopted 1.8 million and 3.8 million tetrahedral grid cells with
294 fine and coarse grid resolutions, respectively. Then, we selected the measured vertical
295 profiles of normalized velocity (V/u_s, u_s = 0.14 m/s means the supply air velocity) and
296 temperature ($\theta = (T-T_s)/(T_e-T_s)$) at Pole 2 and Pole 4 to validate CFD results, where T_s
297 and T_e are the temperatures respectively at diffuser and main exhaust at the normalized
298 height (Z/H, H = 2.72 m is the height of the inpatient ward).

299

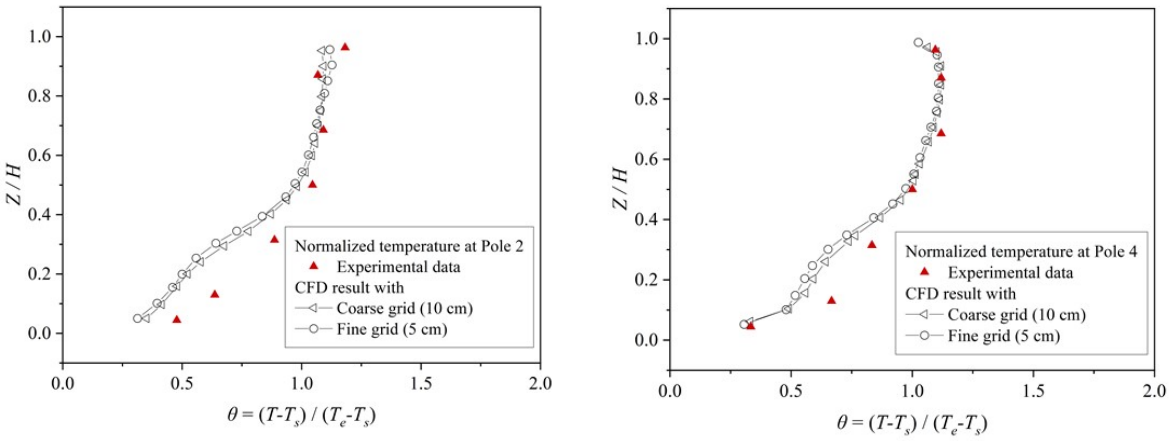

(a)

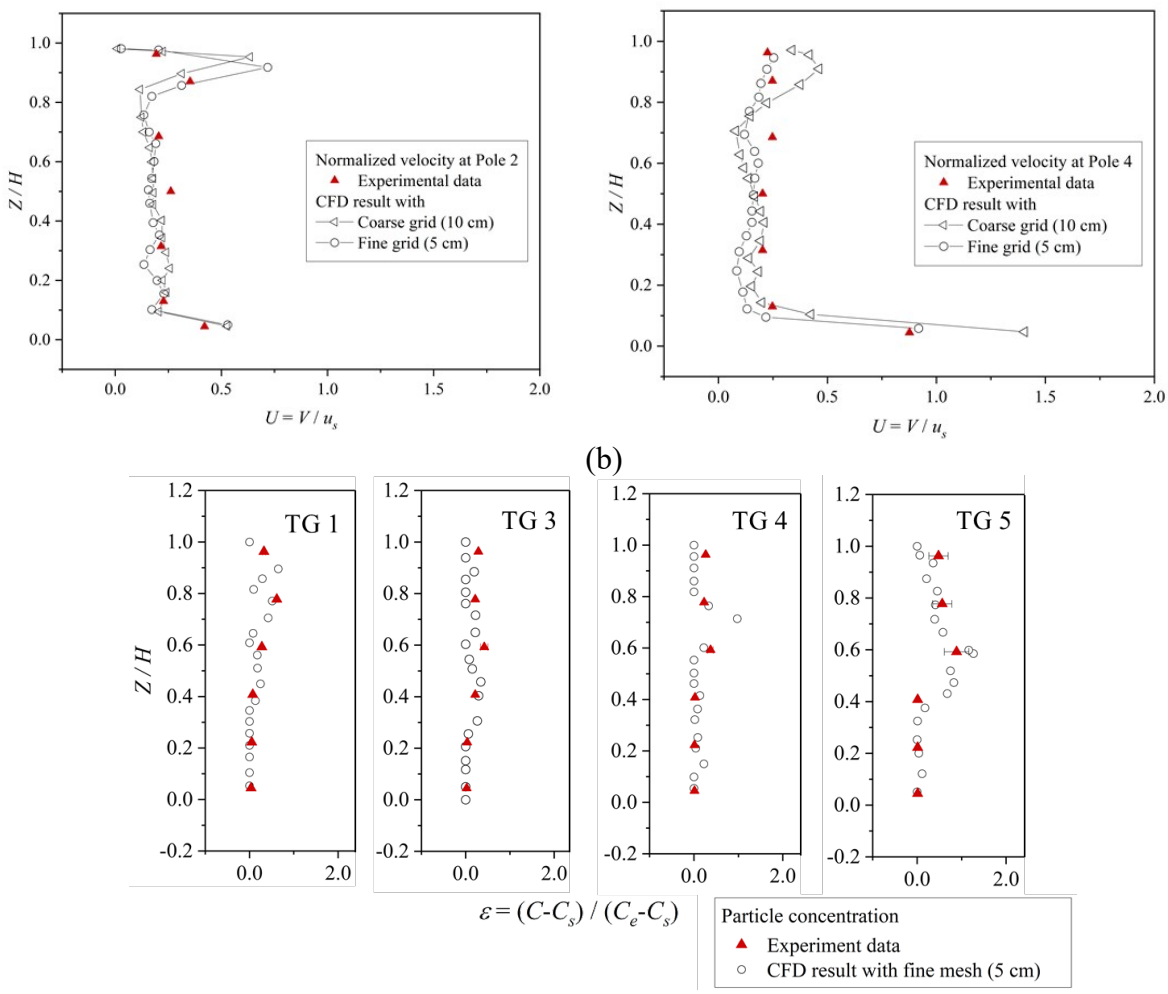

Fig. 3. Vertical profiles of experiment and CFD simulation at Pole 2 and Pole 4 (a) Normalized temperature, (b) Normalized velocity; (c) Normalized 1 μm particle concentration at TG 1, TG 3, TG 4 and TG 5.

300

301 Fig. 3a-b illustrate that CFD results of velocity and temperature agree well with
302 the experimental data. Compared with the coarse grid resolution, fine grid resolution
303 performs better, especially in the velocity at height of Z/H =0.8. Fig. 3c-f display the
304 experimental data and CFD simulation results of normalized particle concentration ε at
305 TG1, TG3, TG4 and TG5 ($\varepsilon = (C\text{-}C_s)/(C_e\text{-}C_s)$, where C, C_s and C_e are the particle
306 concentrations at the measuring location, ventilation supply inlet and ventilation
307 exhausts, respectively). Particles with a diameter of 1 μm are released from the patient's

mouth. In order to quantify the reliability of the validation, we calculated the normalized mean square error (NMSE) and fractional bias (FB), whose ranges were respectively 0.3 to 1.3 and 0.01 to 0.27, which satisfied the recommended criteria ((NMSE$\leqslant$1.5, 0.3 $\leqslant$ FB $\leqslant$ 0.3) in Yang et al [57]. The results indicate that CFD simulation results can reasonably predict the dispersion tendency of indoor particles.

3. Results

3.1. Flow pattern and tracer gas dispersion under various ACH

Our previous study [11] only considered the tracer gas dispersion under the measured mean ventilation condition. In the present study, we emphasize the flow pattern and tracer gas dispersion under different ventilation conditions (i.e., ACH = 0.62, 2.27 and 5.66 h^{-1}).

In order to describe the flow pattern and tracer gas dispersion more clearly, seat locations are shown in Fig. 4a: 13 rows (Row 1-13) and 5 columns (Column A, B, C, D, E) of seats in the passenger cabin. We regard the 1st to 4th rows as the bus front, the 5th and 8th rows as the bus middle and the 9th to 13th rows as the bus rear. The index patient is located at seat 12D (Row 12, Column D, scarlet).

Fig. 4a indicates that when the bus speed is high (ACH = 5.66 h^{-1}), the fresh air enters the skylight inlet at the rear roof, then mixes with the dirty air and moves from the rear to the front. Finally, the mixed air leaves through the outlet at the front roof of the bus. There are body thermal plumes which lead to significant upward airflow near and above human bodies (Fig. 4b). The upward airflow will intertwine with the main flow field and subsequently affect the droplet dispersion. Fig. 4c displays that the

airflow exhaled by the index patient first moves forward, then rises up and finally deflects backward to the bus rear. As depicted in Fig. 4d, the body thermal plumes are most obvious under idling condition (ACH = 0.62 h^{-1}). The ventilation flow from bus rear to bus front enhances significantly as ACH rises with the increasing bus speed (Fig. 4e).

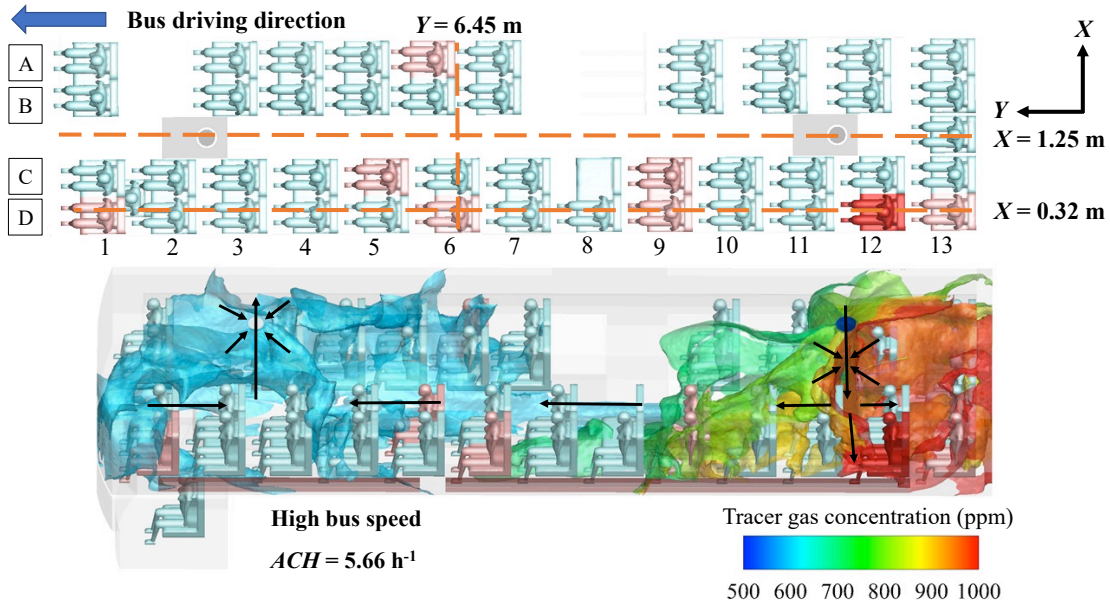

(a)

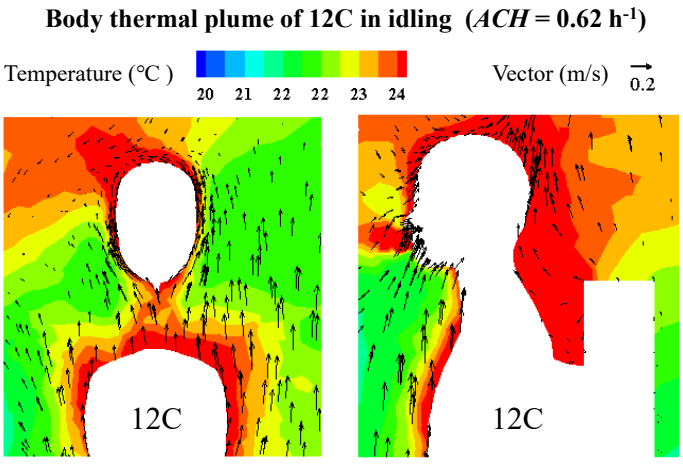

(b)

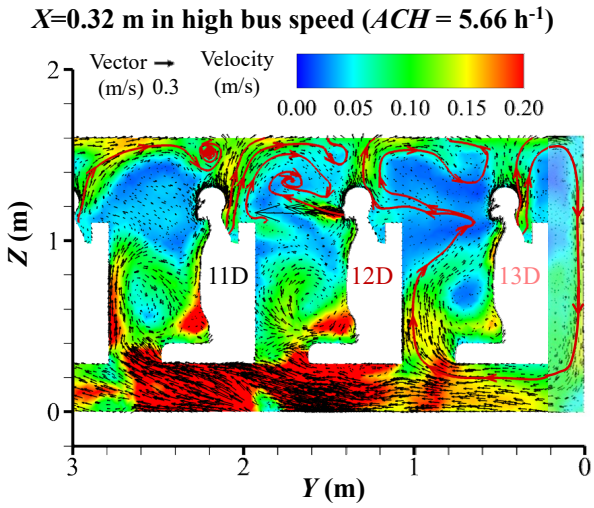

(c)

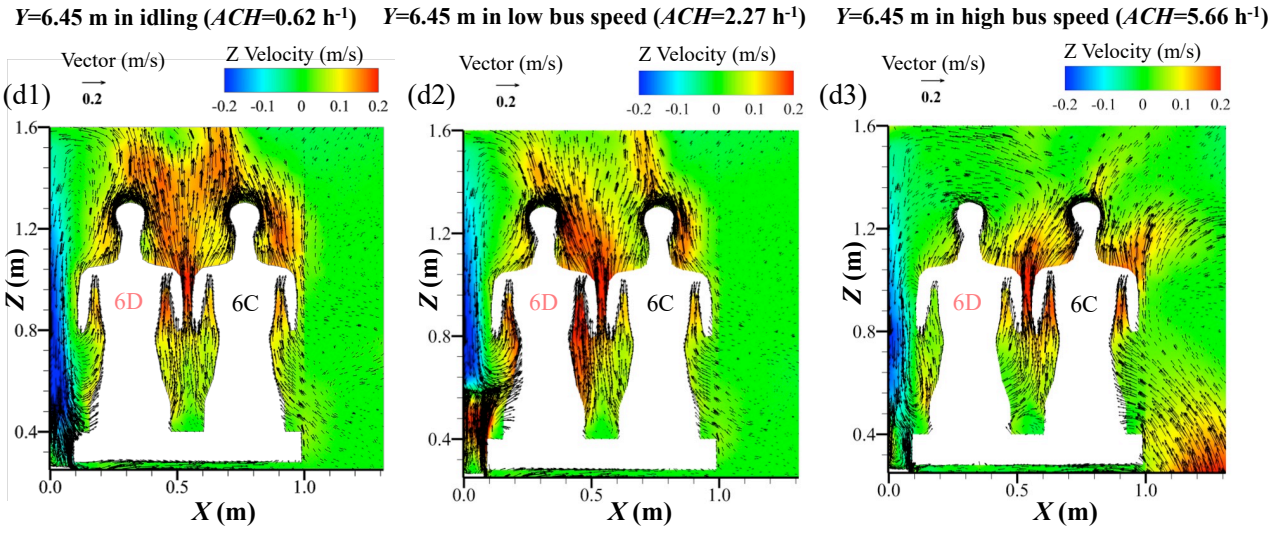

(d)

(e1) **X = 1.25 m in idling (V_{Bus} = 0 km/h, ACH = 0.62 h^{-1})**

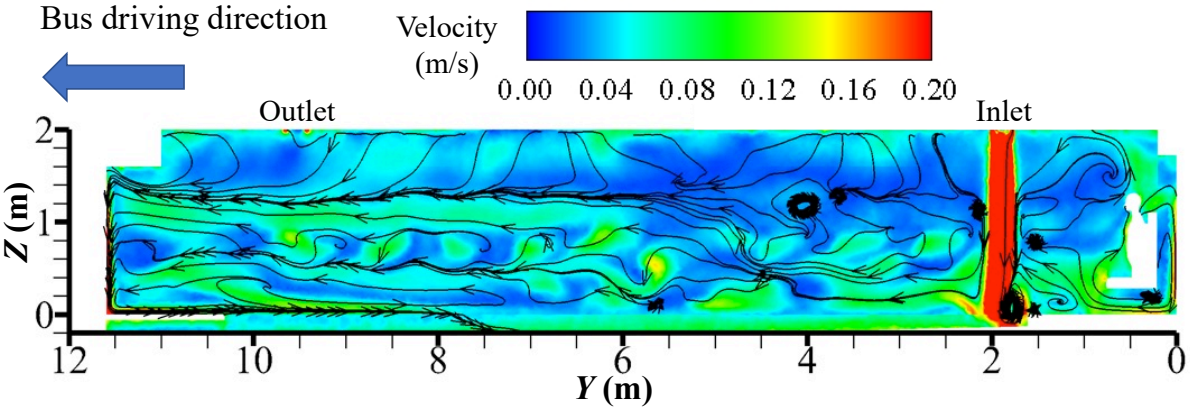

(e2) **X = 1.25 m in low bus speed (V_{Bus} = 30 km/h, ACH = 2.27 h^{-1})**

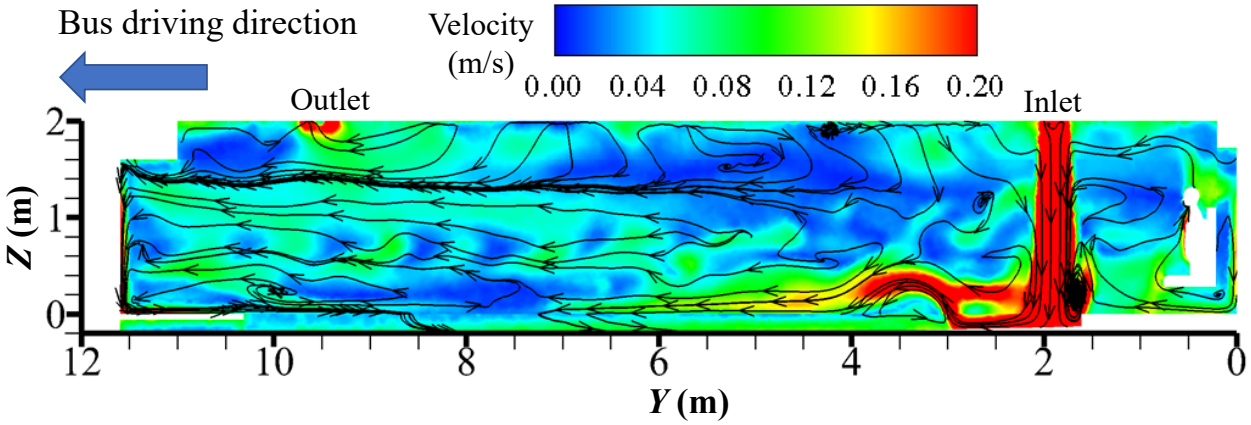

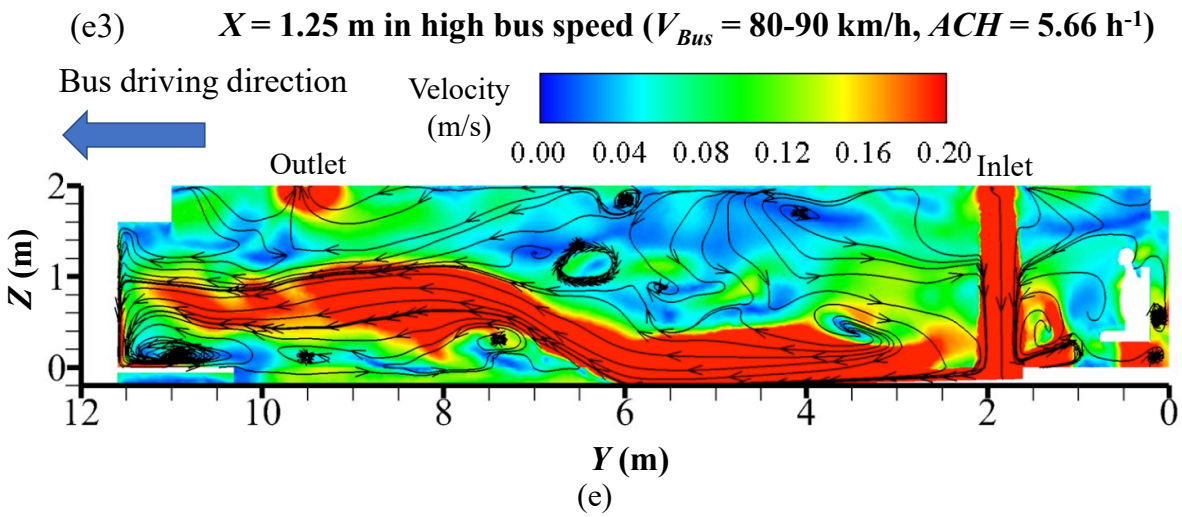

Fig. 4. (a) Cross-section line and general flow characteristics; (b) Body thermal plume of 12C at state of idling; (c) Flow field near index patient at state of high bus speed; Flow field in Plane: (d) Y = 1.35 m; (e) X = 1.25 m. 1-3: idling, low bus speed, high bus speed, respectively.

337

338 Fig. 5 presents the tracer gas concentration distribution of the cross-section at the
339 height of passengers' noses (Z = 1.16 m) under different ACH. Tracer gas concentration
340 in the bus decreases obviously when ACH increases. High tracer gas concentration
341 mainly appears in the bus rear (Rows 9-13), especially at the index patient's side
342 (Columns C and D). Particularly when ACH = 0.62 h^{-1}, the concentration near the index
343 patient is about 7000 ppm, and 5000 ppm in the bus front and middle (Rows 1-8) (Fig.
344 5a). When ACH = 5.66 h^{-1}, the concentration near the index patient is about 1200 ppm,
345 while around 600 ppm in the bus front and middle. (Fig. 5c).

346

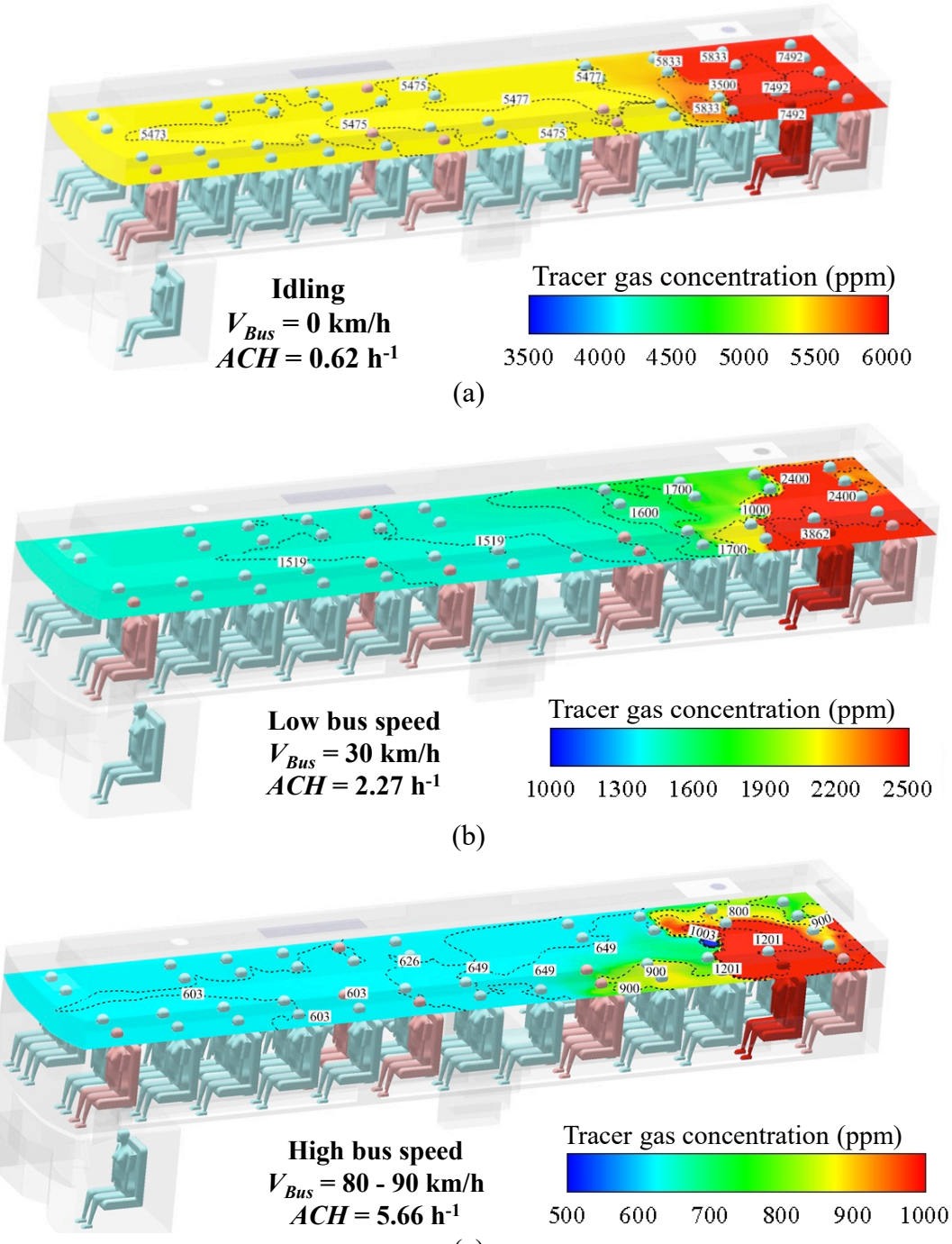

Fig. 5. Tracer gas concentration at state of: (a) idling, (b) low bus speed; (c) high bus speed.

347

3.2. Impacts of RH, ACH and initial diameters on droplet dispersion

3.2.1. Impacts of RH on droplet evaporation and transmission

Fig. 6 displays the temporal variation of droplet diameters (droplet evaporation history) under different *RH* (35%, 95%) when initial diameter d_p is 50 μm and 100 μm. When d_p = 5 μm, droplets can evaporate into 1.83 μm nuclei within 0.1 s under both *RH* conditions, so we don't show its evaporation process here. The results confirm that 50 μm droplets can evaporate into 18.26 μm droplet nuclei in 1.3 s under *RH* = 35% and 2.1 s under *RH* = 95%. However, it takes 5 s for 100 μm droplets to evaporate into 36.50 μm nuclei under *RH* = 35% and longer time (> 6 s) under *RH* = 95%. Although droplets take a longer time to evaporate in more humid environment, the overall impact of *RH* is not significant in this coach bus with complicated interactions of ventilation airflow and thermal body plumes (Fig. S1).

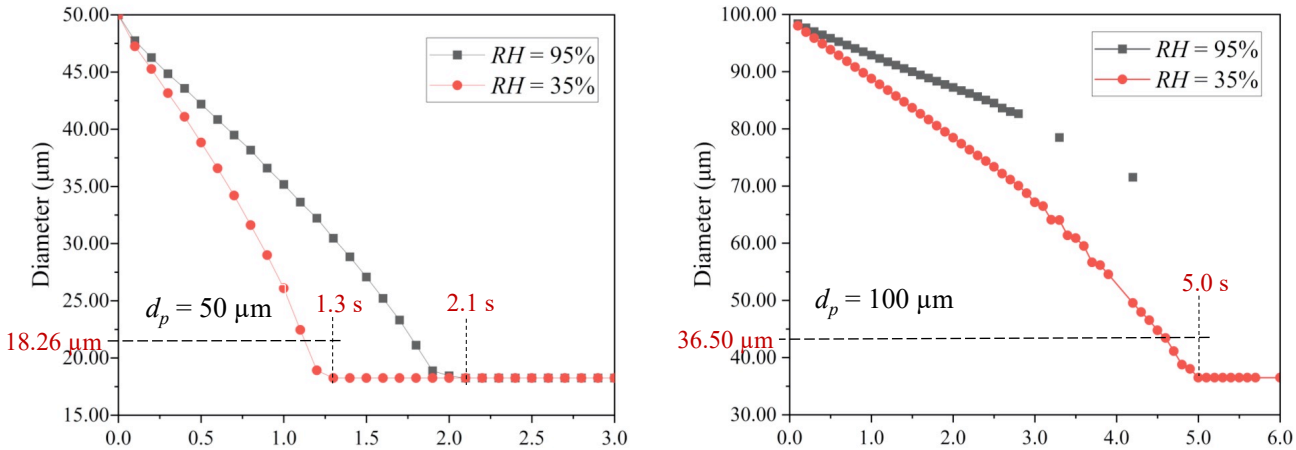

Fig. 6. Temporal variation of droplet evaporation (dp = 50 μm, 100 μm; RH = 35%, 95%).

3.2.2. Impacts of ventilation rates on droplet dispersion

We have investigated the impacts of ventilation rates on the dispersion of droplets in different initial diameters (5 μm, 50 μm and 100 μm), and find that the dispersion mechanism is more affected by the gravity force and less influenced by the ventilation airflow for larger droplets. Thus, to better reveal the influence of ventilation rates, we only select 5 μm droplets to display their distribution under RH = 35% at t=5s, 30 s, 60 s and 300 s with three ACH, as shown in Fig. 7.

As verified in Fig. 7a1-b1, after being exhaled by the index patient, droplets first move forward due to the initial exhalation flow, then rise up following the upward flow near the index patient, and spread with the main airflow routes (Fig. 7a2-b2). Due to the variation in ventilation rates, the spatial distribution of droplets also differs significantly (Fig. 7a3-a4). When ACH = 5.66 h^{-1} with larger supply airflow blowing to the bus front, more droplets move forward and escape from the skylight outlet, leaving relatively fewer droplets in the bus rear (Fig. 7a4-b4). The results show that increasing the ventilation rate is beneficial to droplet dilution and excretion, and significantly reduces the droplet concentration near the index patient (i.e., seats 11D, 12C and 13D).

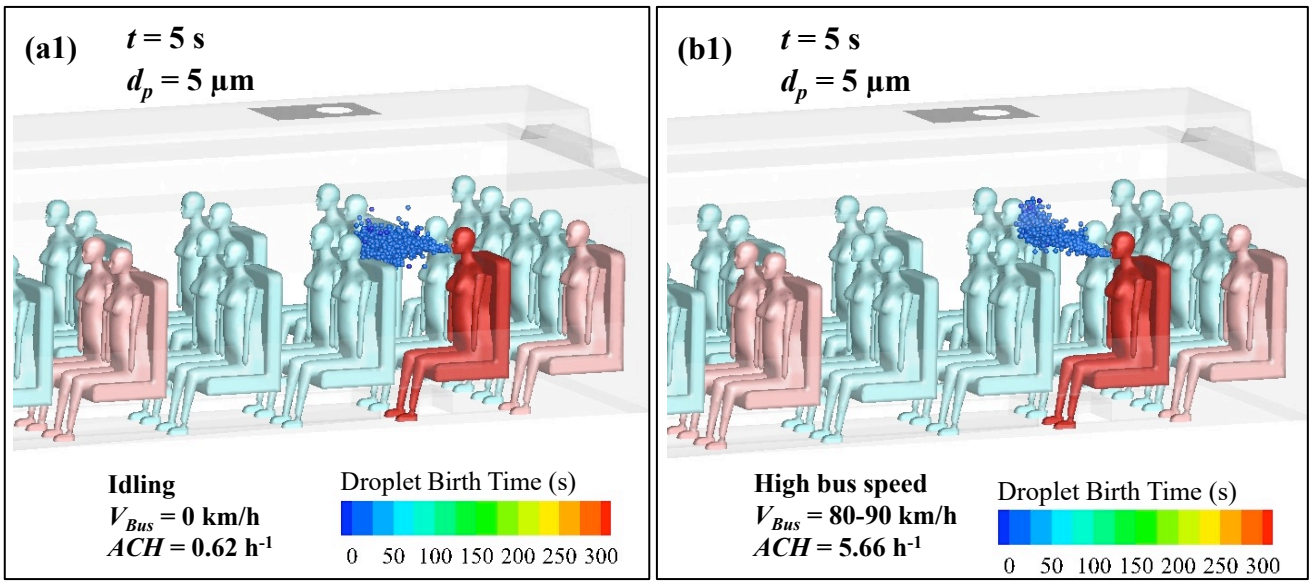

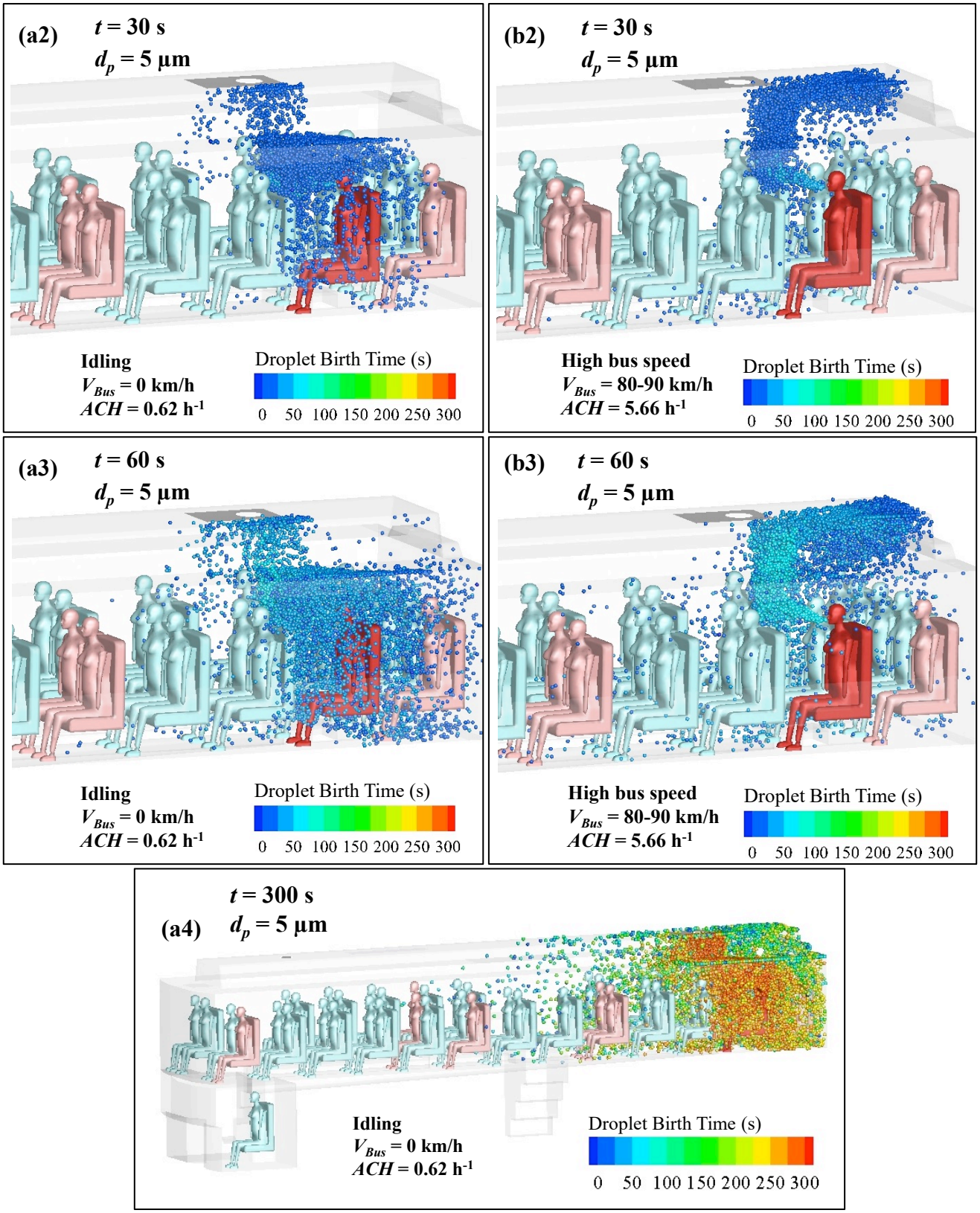
(a2)
t = 30 s
d_p = 5 µm
Idling
V_Bus = 0 km/h
ACH = 0.62 h-1
Droplet Birth Time (s)
0 50 100 150 200 250 300
(b2)
t = 30 s
d_p = 5 µm
High bus speed
V_Bus = 80-90 km/h
ACH = 5.66 h-1
Droplet Birth Time (s)
0 50 100 150 200 250 300
(a3)
t = 60 s
d_p = 5 µm
Idling
V_Bus = 0 km/h
ACH = 0.62 h-1
Droplet Birth Time (s)
0 50 100 150 200 250 300
(b3)
t = 60 s
d_p = 5 µm
High bus speed
V_Bus = 80-90 km/h
ACH = 5.66 h-1
Droplet Birth Time (s)
0 50 100 150 200 250 300
(a4)
t = 300 s
d_p = 5 µm
Idling
V_Bus = 0 km/h
ACH = 0.62 h-1
Droplet Birth Time (s)
0 50 100 150 200 250 300

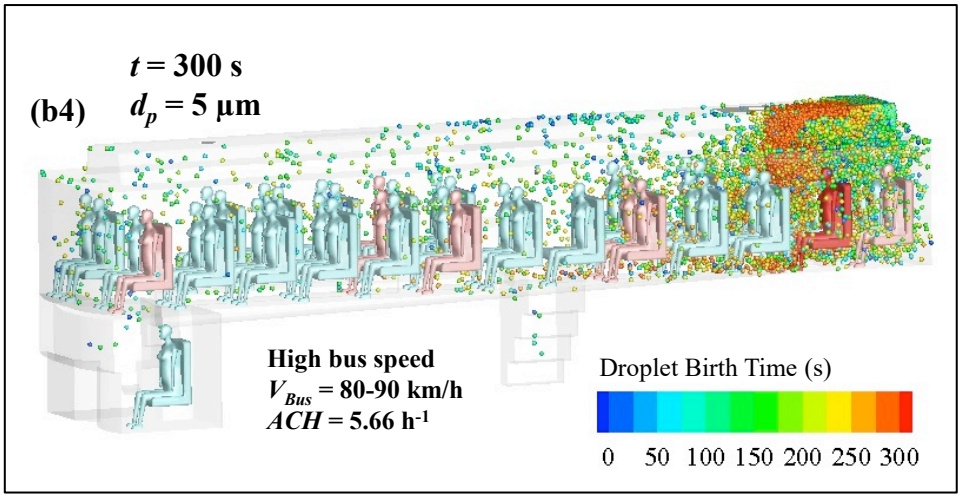

Fig. 7. Distribution of 5 μm droplets with *RH* = 35% at state of: (a) idling, (b) high bus speed.

378

379 ***3.2.3. Impacts of droplet initial diameters on droplet dispersion***

380 Fig. 8 indicates the evaporation and dispersion of droplets with different initial
381 diameters when *RH* = 35% and *ACH* = 2.27 h^{-1}. 5 μm droplets can evaporate rapidly
382 into nuclei, so they are more significantly affected by the airflow field, and spread wider
383 in the whole bus (Fig. 8a1-a3). Due to the combined action of airflow pattern and
384 gravity force, 50 μm droplets mainly concentrate at the bus rear (Fig. 8b1-b3). With the
385 dominance of gravity force, 100 μm droplets rapidly settle down from the exhalation
386 jet after being exhaled from the index patient's mouth (Fig. 8c1-c3). Basically, the larger
387 the initial diameter is, the quicker the droplets deposit, and hence the smaller range they
388 propagate and the more they remain in the bus.

389

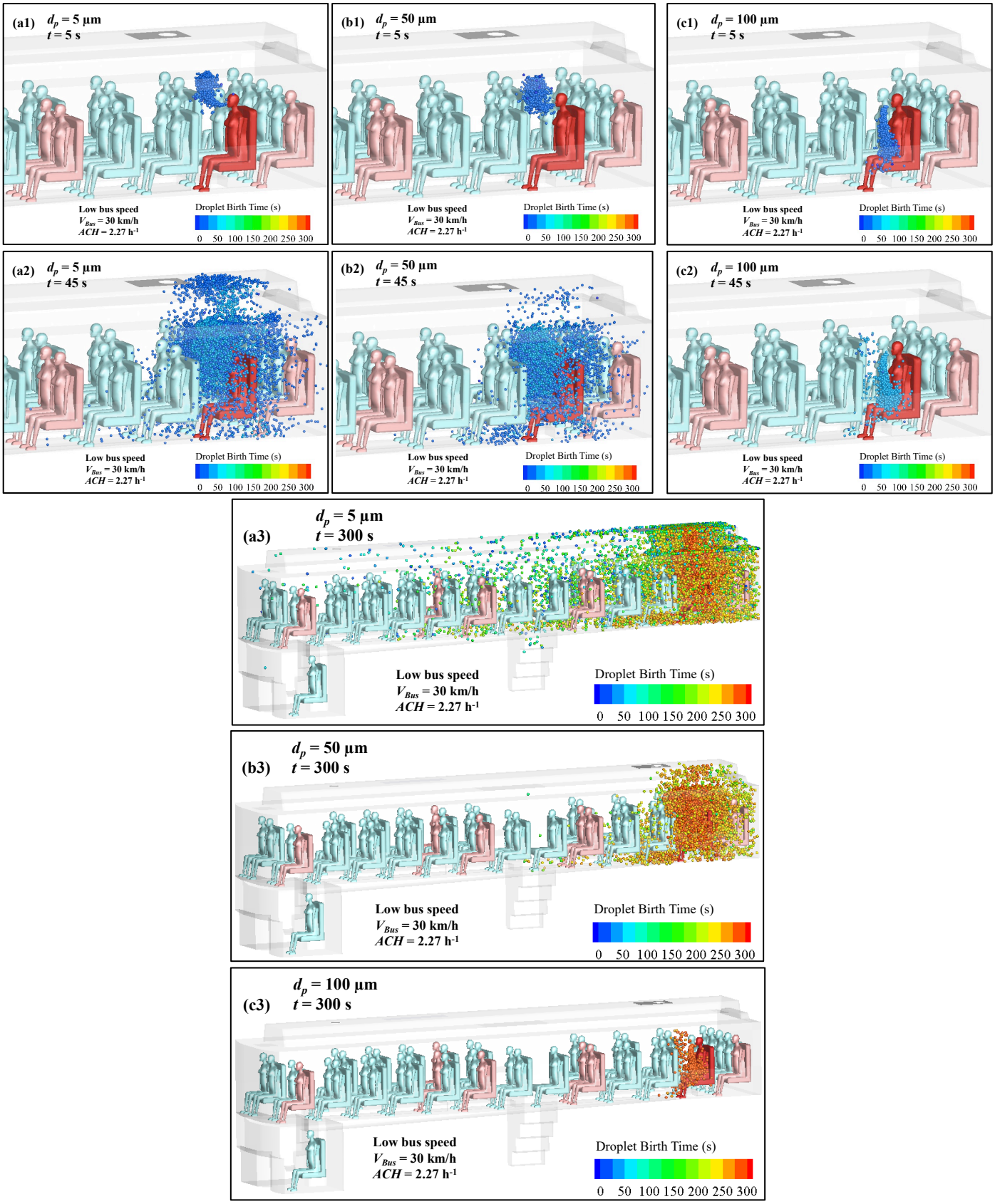

Fig. 8. Droplets distribution in low bus speed with RH = 35%: (a)d_p = 5 µm, (b) d_p = 50 µm, (c) d_p = 100 µm.

3.3. Intake fraction and infection risk of each passenger

Fig. 9 depicts the 30-minute-exposure intake fraction (*TIF*) of each passenger which is defined as dividing the number of droplets a passenger inhaled by the total number of droplets released from the index patient (360,000). Fig. 10 depicts the 30-minute-exposure infection risk (*TIR*) of each passenger which is calculated by Wells-Riley equation (Eq. (9)). The *X*-axes represent the row of each passenger, where 12D is the location of the index patient and 8C is unoccupied. Passengers without data indicate that they did not inhale PLD released by the index patient.

For 5 μm droplets, the ventilation rates influence the *TIF* and the subsequent *TIR*, with a higher ventilation rate leading to more passengers at *TIR*. When ACH = 0.62 h^{-1}, only few 5 μm droplets are inhaled by passengers in the bus front (Fig. 9a), leading to most front passengers at no droplet *TIR* (Fig. 10a). When ACH increases to 5.66 h^{-1}, even more front passengers are at *TIR*, and both *TIF* and *TIR* of passengers decrease with the distance between the passenger and index patient (Fig. 9c). Although 5 μm droplets disperse more widely with the increasing ventilation, the *TIR* is quite low (<0.01%) for front passengers. Regardless of ventilation rate, more than 97% of 50 μm droplets deposit near the index patient due to gravity (Table. S1), so only the middle and rear passengers are at *TIR* with the highest infection risk for passenger 12C (3.13% under ACH = 5.66 h^{-1}) (Fig. 10b). While for 100 μm droplets, over 99.5% of them deposit locally due to gravity (Table. S1), making nobody at *TIF*, so we don't display the infection risk.

For the tracer gas, a higher ventilation rate leading to lower *TIR*. The *TIR* is 11.10-15.29% under ACH = 0.62 h^{-1}, and decreases to 1.27-3.09% when ACH = 5.66 h^{-1} (Fig.

413 10c). The *TIR* of tracer gas for each passenger is more uniform and distinctly higher

414 under the same condition, compared with that of droplets.

415

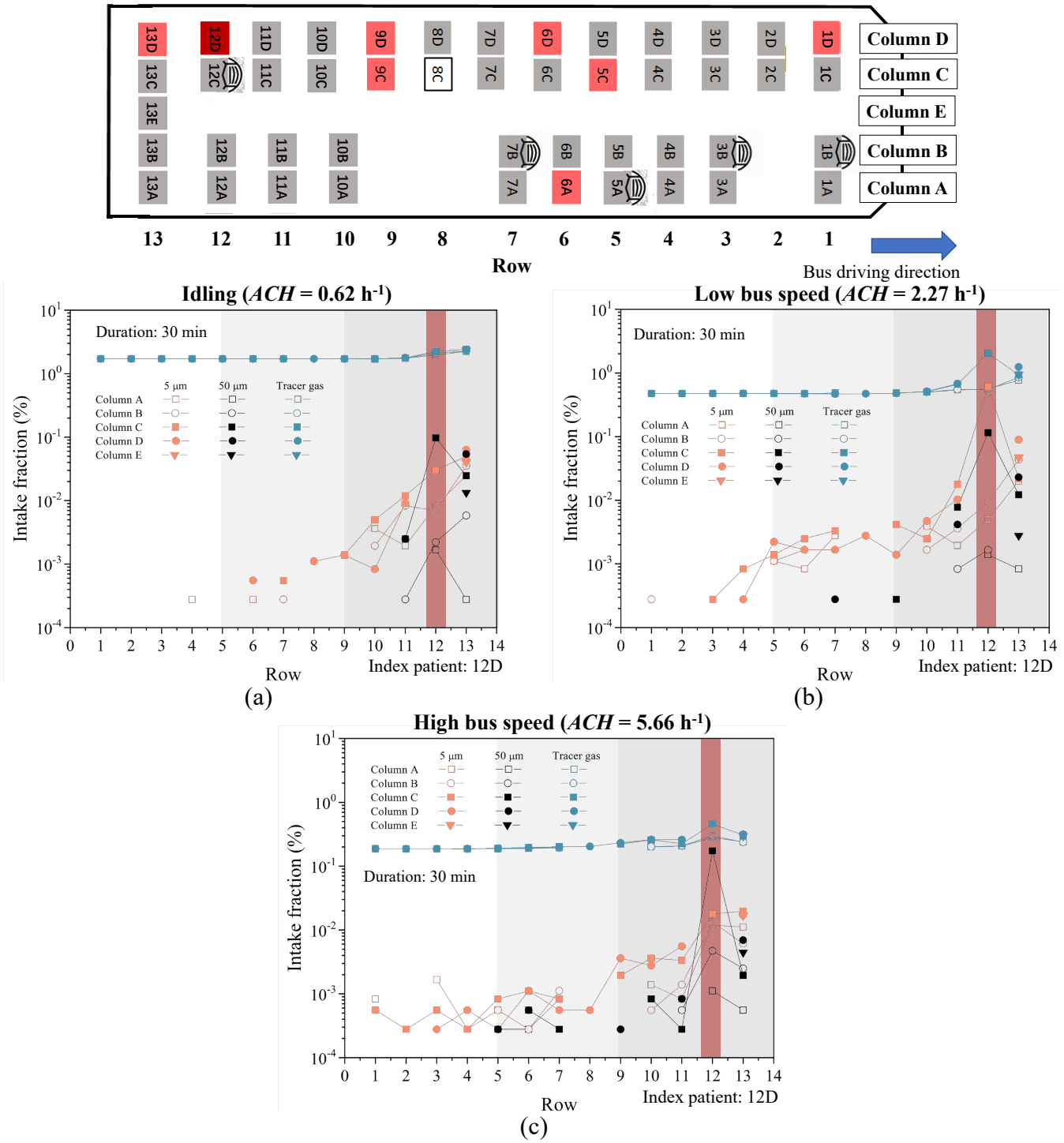

Fig. 9. Intake fraction of each passenger in a duration of 30 min under *RH* = 35% at state of: (a)idling, (b) low bus speed, (c) high bus speed.

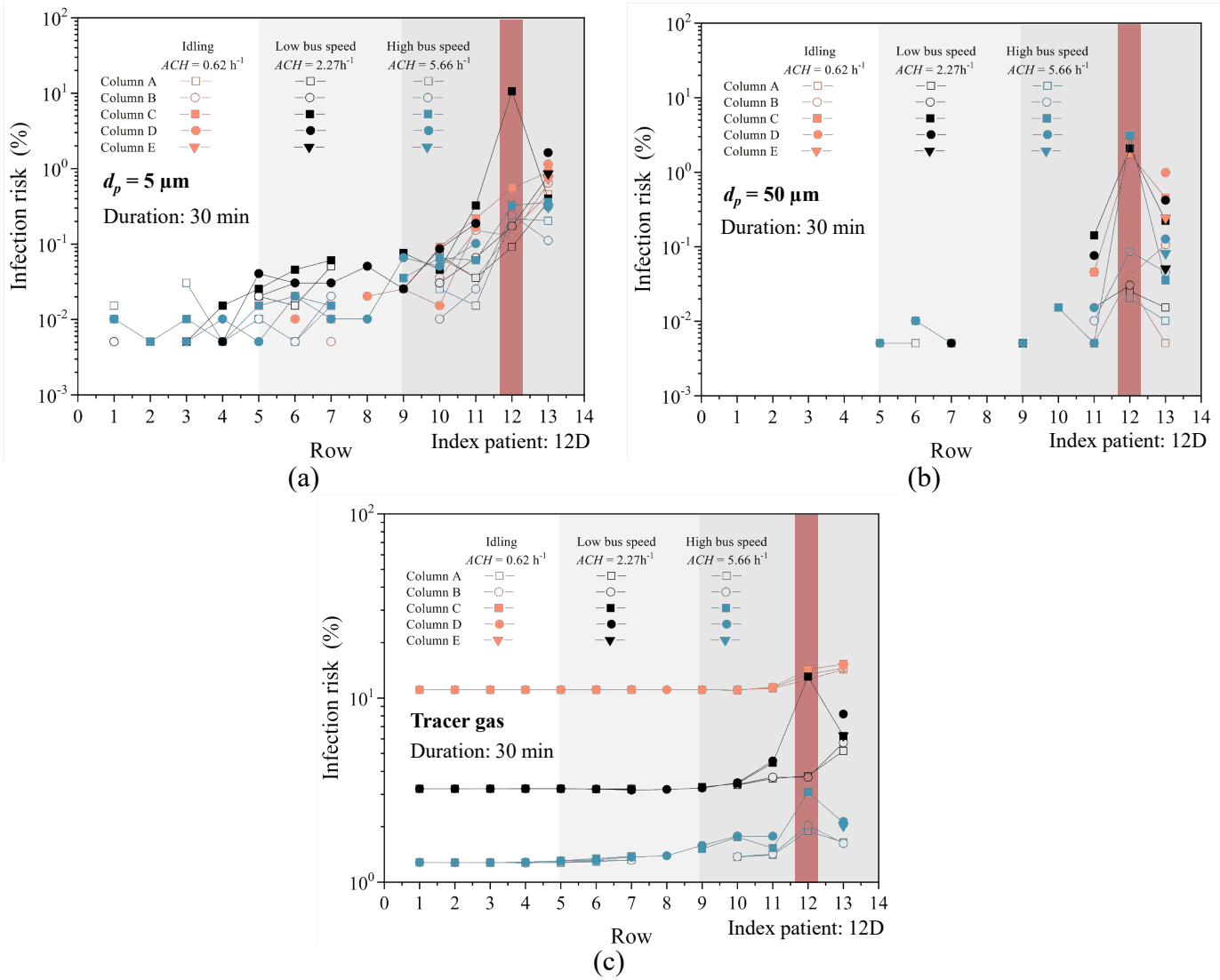

Fig. 10. Infection risk of each passenger under RH = 35%: (a)d_p = 5 μm, (b) d_p = 50 μm, (c) tracer gas. (Note: infection risk within 30 min was calculated.)

3.4. Infection risk of each passenger in this epidemic outbreak

The total duration of the bus journey is 200 min, and the passenger seating arrangement and driving route are depicted in Fig. 11a. We adopted the calculated 30-minute simulation results to infer the quanta of virus-laden droplets or tracer gas inhaled by each passenger throughout the whole journey. Fig. 11b-11d display the whole-

journal-exposure infection risk (*WIR*) of passengers (except the index patient at seat 12D). Note that the logarithmic coordinate system is employed in Fig. 11c-11d.

Under all conditions, the highest *WIR* of the tracer gas, 5 μm and 50 μm droplets occurs at seat 12C with 33.85%, 16.99% and 17.40%, and followed by seat 13D with 24.97%, 4.28% and 1.57%, respectively. It can be seen from Fig. 11 that the *WIR* of front-seat passengers significantly decreases with the increasing initial droplet diameter. However, passengers near the index patient (i.e., seats of 11D, 12C and 13D) are always at comparatively high *WIR*.

For the tracer gas (Fig. 11b), the *WIR* of front passengers is relatively even at ~14.00%. For 5 μm droplets (Fig. 11c), the *WIR* is quite discrepant for passengers at different locations, and is less than 0.15% for the front passengers (Rows 1-4), while up to 16.99% for the passenger at 12C. For 50 μm droplets (Fig. 11d), no front passengers are at *WIR*.

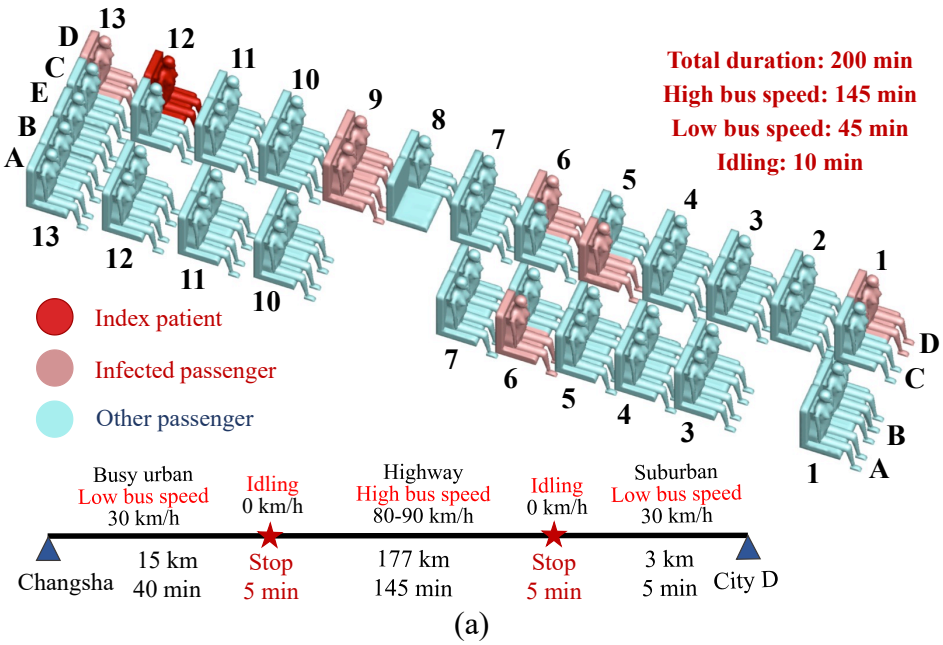

(a)

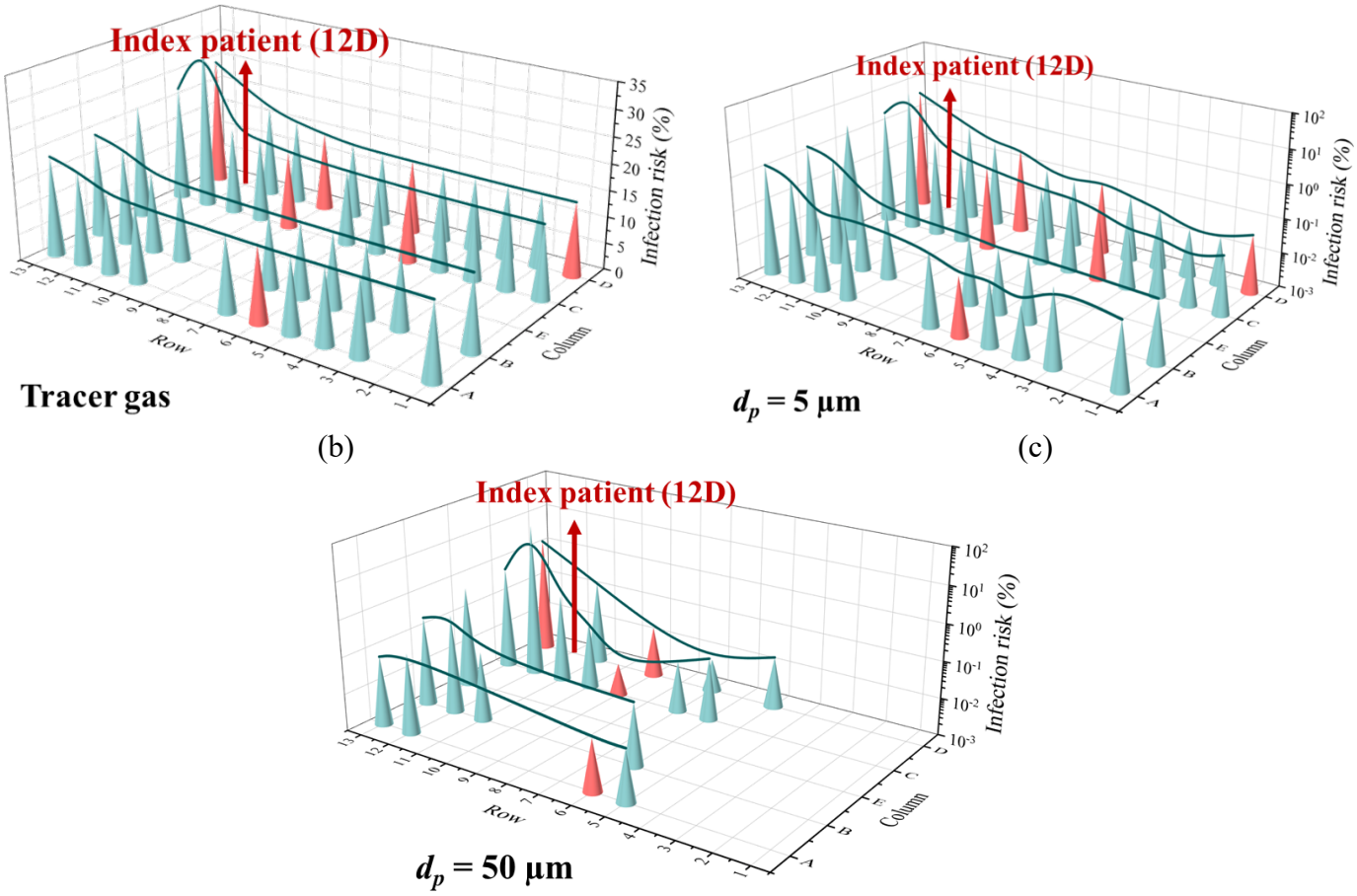

Fig. 11. (a) Seating arrangement, journeys, and distribution of index patient and infected passengers, (b) Tracer gas, (c) d_p = 5 μm, RH = 35%, (d) d_p =50 μm, RH = 35%. (Note: infection risk is calculated based on this epidemic case.)

4. Discussion

4.1. The unique airflow field characteristics of the coach bus

The strength of this study lies in the investigation of the combined effect of the indoor main airflow and human thermal plumes on the airflow field in this unique in-coach environment. The coach bus only has small roof-opening skylight suppliers to open up for fresh air, but no windows are openable. Fig. 12 depicts the external surface wind pressure coefficient around the running bus. It shows that the pressure on the rear half is higher than the front half of the bus, which leads the air enter the bus from the

443 rear skylight and exit from the front, i.e., the indoor main airflow is moving from the
444 rear to front. This unique rear-to-front airflow pattern makes the pathogen-laden
445 expiratory droplets propagate the entire bus when the index patient is seated at the bus
446 rear (12D) and hence results in large-scale transmission in this outbreak, as was also
447 found in Mesgarpour et al. [58]. If the index patient was in the middle or front of the
448 bus, the rear of the bus will be a low-risk area [59].

449

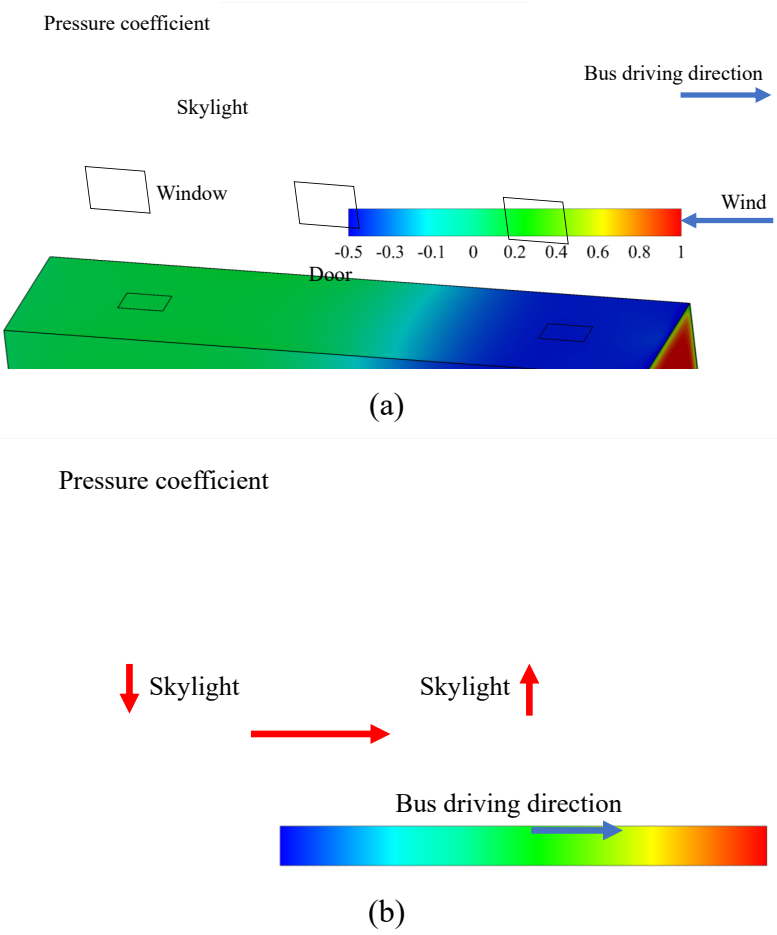

Fig. 12. (a) Pressure coefficient distribution on bus surfaces, (b) External pressure coefficient distribution of bus.

450

Besides the main airflow, the body thermal plumes cannot be neglected in the crowded coach bus, as they can cause an upward airflow near each human body and hence influence the droplet dispersion in the respiratory region—the last few inches for aerosol transmission to effectuate [17, 22, 60]. Meanwhile, Yang et al. [61] found that strong main airflow could destroy the thermal plumes. The body thermal plumes are obvious under the small background velocity field and can inhibit droplets from entering the respiratory area. This certain protective effect makes droplet infection risk stay low under ACH = 0.62 h^{-1}. However, the body thermal plumes will be disturbed with the enhancement of the main airflow, leading to an increase of the droplet infection risk under ACH = 2.27 h^{-1}.

4.2. Impacts of RH and initial droplet diameter on droplet dispersion

Redrow et al. [38] demonstrated that 10 μm droplets could evaporate completely in 0.25 s at RH = 20% and 0.55 s at RH = 80%, and RH influenced 0.4-10 μm droplet transport in a simulated room where the mean air velocity was almost zero. Liu et al. [17] revealed that 100 μm droplets took more than 100 s to evaporate at RH = 95% and <2 s at RH = 35%, which made 100 μm droplet dispersion totally distinct under different RH in an empty room. However, our study achieved a completely different finding: RH rarely influences the droplet (5-100 μm) dispersion in the coach bus. The possible reason may lie in the complex indoor environment of the coach bus which is different from those in the above literature. In our study, we found that the interaction of the main airflow and body thermal plumes made the airflow much more complex, which significantly influenced the droplet/tracer gas dispersion. Moreover, Chen and Zhao [62]

and Xie et al. [33] indicated that regardless of the *RH*, small droplets evaporated completely quickly, and big droplets deposited downward immediately before fully evaporating due to gravity dominance. Therefore, there was a tiny difference of droplet ultimate fates and infection risk between different *RH* (Table. S1, Fig. S2), which agreed well with the study on coach bus conducted by Yang et al. [28].

The droplet diameter is the fundamental property that determines its transport characteristics. The transport behavior of a droplet depends on its interaction with the surrounding gas molecules, as well as the force acting on it [63]. When the droplet diameter increases, its dominant influencing mechanism changes into gravity force or drag force [64, 65]. Zhu et al. [66] indicated that the droplets of 30 μm or smaller were mostly influenced by indoor airflow, but those of 50 – 200 μm were significantly affected by the gravity force. Our study found that small droplets (i.e., tracer gas and 5 μm droplets) can follow the airflow and spread throughout the cabin, while large droplets (i.e., 50 μm and 100 μm) deposited near the index patient due to the dominant gravity force. Namely, small droplets can travel farther than large droplets, leading to a larger range of inhalation transmission.

When the droplet is small enough, the behavior of the droplets and the surrounding gas requires the kinetic theory of gases. Therefore, tracer gas was adopted as a surrogate for droplets and droplet nuclei smaller than 5 μm in general room environments, which had been verified by existing studies [36, 44, 67]. However, unlike general rooms, buses are longer and narrower in shape (11.4 m long and 2.5 m wide in our study) with more obstacles (i.e., human bodies and seats), which provides much more surface for droplets to deposit. Our study verifies that most droplets deposit on the route through the long-

496 and-narrow bus so that only a small fraction can spread to the bus front. Therefore,
497 passengers in the bus front can expose to few droplets and lead to a quite low infection
498 risk. However, tracer gas does not deposit and can disperse in the whole cabin, resulting
499 in distinctly higher infection risk under the same condition. Hence, tracer gas cannot be
500 utilized to mimic the dispersion processes of droplets which can be deposited on the
501 surfaces. Meanwhile, Zhao et al.[68] indicated that the deposition of 0.7 μm particles
502 was insignificant in an aircraft cabin. Lai and Nazaroff [69] reported that droplets in the
503 range of 0.1-0.2 μm has the lowest deposition rate in indoor environments. Hence, we
504 conclude that tracer gas can only be adopted to simulate the dispersion of fine droplets
505 (e.g., 0.1-0.7 μm) with little deposition in coach buses.

506 ***4.3. Impacts of ventilation rates on droplet dispersion and infection risk***

507 van Doremalen et al. [6] have found that the SARS-CoV-2 virus can remain
508 infectious in aerosols for hours and up to days on surfaces, leading to probable
509 transmission. Among the three main transmission routes, the aerosol inhalation route is
510 predominant and can occur over a long distance when the ventilation is insufficient [64,
511 70]. Therefore, this study aims to investigate the mechanism of factors affecting the
512 aerosol inhalation transmission and infection risk in a crowded coach bus.

513 Enhancing the indoor ventilation rates can promote dilution and removal of
514 pathogen-laden expiratory droplets or droplet nuclei, and hence reduce the infection
515 risk [10, 67, 71]. Our study also confirms that the infection risk is closely related to
516 ventilation rates. When the ventilation rate is small, droplets can only disperse in the
517 bus rear and middle. Larger ventilation airflow drives droplets to disperse more widely
518 in the bus, but the infection risk is relatively low in the bus front (lower than 0.1% when
519 ACH = 5.66 h^{-1} for 5 μm droplets). While for tracer gas, the inhalation infection risk can

520 be reduced by an order of magnitude as *ACH* increases from 0.62 h^{-1} to 5.66 h^{-1}. Thus,
521 for the large range of initial diameters of respiratory droplets, the infection risk
522 decreases with the increasing ventilation rates.

523 The World Health Organization [72] has indicated that the long-range aerosol
524 inhalation transmission of COVID-19 is opportunistic in specific settings, particularly
525 in crowded and inadequately ventilated indoor environments. Li et al. [10] revealed the
526 long-range aerosol inhalation transmission in an insufficient ventilation restaurant and
527 the longest transmission distance is 4.6 m. In this outbreak, the coach bus was supplied
528 at a time-average ventilation rate of 1.72 L/s per person [11] far lower than the
529 ASHRAE Standard (2019) [73], leading to long-range aerosol inhalation transmission
530 with a longest distance of 9.46 m between the index patient and the infected passenger
531 (1D). Both simulation results and actual outbreak confirm the important role of
532 ventilation on aerosol inhalation transmission and infection risk.

533 ***4.4. Infection risk in realistic bus outbreak***

534 Another merit of this study lies in that we utilized the real outbreak data to back-
535 calculate the infection risk of each passenger according to the bus speeds and the
536 corresponding exposure time in this COVID-19 outbreak inside the coach bus. Based
537 on the numerical calculation results, we explained the following three characteristics
538 for the spatial distribution of infected passengers in this realistic epidemic: (1) more
539 infected passengers in the middle and rear of the cabin (six in Row 5-13) than in the
540 front (only one in Row 1-4); (2) more infected passengers on the index patient side (six
541 in Column C-D) than on the opposite side (only one in Column A-B).

542 The trajectory of droplets is determined by the airflow pattern, gravity force, and
543 the process of evaporation in terms of their diameter. 50 μm droplets can transmit a

544 short distance and then gradually deposit due to the gravity force, so only part of them
545 can be inhaled by passengers in the rear and middle, which leads to short-range aerosol
546 inhalation transmission [7]. Meanwhile, smaller droplets ($\leqslant$ 5 μm) can continue
547 spreading to the bus front, leading to both short and long-range aerosol inhalation
548 transmissions. Thus, the infection risk is higher near the index patient and decreases
549 with distance, namely, more passengers in the middle and rear were infected than those
550 in the front.

551 Higher infection risks for both tracer gas and droplets are found on the index
552 patient's side (Column C and D). The reason may lie in the cold "gravity current" [74]
553 falling to the cabin floor and spreading throughout the entire cabin, established by the
554 skylight inlet above the aisle near the index patient. The cold "gravity current" then rose
555 with the body thermal plume of each passenger and finally exhausted at the bus front
556 skylight outlet. The blockage of the floor-level "gravity current" by the toilet in the
557 lower deck of the cabin made contaminated air spread slightly more to the index patient
558 side than to the opposite side, which brought about a higher infection risk on the index
559 patient side.

560 It can be found that there are some deviations between the realistic location of the
561 infected person and the calculated location of passengers at high infection risk. The
562 reason may lie in the following aspects. Firstly, we have calculated the infection risk of
563 aerosol inhalation transmission for droplets with some representative diameters (tracer
564 gas, 5 μm, 50 μm, and 100 μm). However, the PLD is in the large range of diameters
565 (0.1 - 100 μm) which may highly affect the infection risk. Thus, it needs further study
566 on the infection risk distribution of droplets in large range of diameters. Secondly, there
567 are many other factors that may affect passengers being infected, such as other

568 transmission routes (e.g., direct-contact/indirect-contact transmission [75]), immunity
569 of passengers, the activity status of passengers in the bus (wear a mask or not, speak or
570 not, etc). However, our study quantified the impact of natural ventilation on the
571 infection risk of tracer gas and droplets and provided a basis for the prevention and
572 control of respiratory infectious diseases in coach buses.

573

574 ***4.5. Limitations and future research***

575 There are several limitations of the present research that should be acknowledged.
576 Different respiratory activities, including breathing, speaking, coughing, sneezing, etc,
577 can affect the generation and dispersion of droplets [26, 58, 76]. We only considered
578 the index patient's breathing activity, because the epidemiological survey suggests that
579 the index patient did not cough or talk to anyone during the whole trip. In the future,
580 we will further consider more respiratory activities and more influencing parameters
581 (e.g., natural ventilation modes by opening windows, source location, ambient
582 temperature, different total heat flux for occupant etc). Meanwhile, it deserves further
583 investigation on how the droplet final fates change with various ventilation rates and
584 initial diameters under the combined effect of ambient airflow, gravity and body thermal
585 plumes. Due to the positive pressure at the bus rear and the negative pressure at the bus
586 front, opening the windows at the bus rear is beneficial to increase the ventilation rates,
587 but the specific method needs further evaluation. Additionally, during the epidemic of
588 infectious disease, public vehicles are required to be less than half occupancy in order
589 to reduce the infection risk, which has not only caused great economic losses to the
590 transportation operation companies, but also caused inconvenience to people's travel.
591 Therefore, it is worth further investigating the infection risk under different seat

arrangements to give a more specific suggestion for arranging the occupancy in different coach buses.

5. Conclusions

Based on experiments of one-infecting-seven COVID-19 outbreak with an index patient at bus rear, this paper performed CFD simulations to explore the PLD dispersion and infection risk in a crowded coach bus, which is important but still scarce. The integrated effects of initial droplet diameters, natural air change rates per hour and relative humidity are considered.

Some meaningful conclusions can be stated:

(1) In this bus epidemic, inadequate ventilation, crowded passengers and long exposure time (200 min) are the main reasons for the large number of infected passengers (i.e., seven) with a longest infected distance of 9.46 m.

(2) The pressure difference between the bus rear and front makes the air enter the bus from the rear ceiling-level skylight (inlet), and leave through the bus front ceiling-level skylight (outlet), carrying droplets/tracer gas disperse from the rear to the front. Higher bus speed leads to more ventilation rates.

(3) Tracer gas can only be adopted to simulate fine droplet (e.g., 0.1-0.7 μm) dispersion in coach buses. The gaseous inhalation transmission can occur in the entire cabin, and its infection risk is greatly reduced with the increasig ventilation rates. When ACH increases from 0.62 h^{-1} to 2.27 h^{-1} and 5.66 h^{-1}, TIF of tracer gas for each passenger decreases from 11.10-15.29% to 3.20-13.08% and 1.27-3.09%.

(4) Over 99.5%/97.0% of large droplets (i.e., 100μm/50μm) deposit locally due to gravity. Thus, the *TIF* of 100μm/50μm droplets is almost independent of *ACH*, with a peak *TIF* (~3.1%) near the index patient. Because gravity is less significant for 5 μm droplets which can spread more widely with the ventilation airflow from bus rear to front and disperse even further with the increasing ventilation.

(5) Unlike ordinary rooms, most droplets will deposit on objects when spread in the long-and-narrow bus, but tracer gas will not deposit. therefore, the infection risk of tracer gas is obviously higher than that of 5-100μm droplets.

(6) Relative humidity *(RH*=35% and 95%*)* affects the droplet evaporation process, but insignificantly influences the dispersion and infection risk.

For coach buses and other indoor environments, fresh air should be sufficiently supplied for the occupants. When the occupancy rate of vehicles is high, it is recommended to open windows or ceiling-level skylight at the vehicle rear to attain more fresh air into the bus and better natural ventilation. Even for cold winter or hot summer, we should find a balance between energy consumption and human health, i.e., to ensure thermal comfort by air conditioners or heating devices meanwhile provide sufficient external fresh air by opening ceiling-level skylight or small-area windows to reduce the infection risk in the vehicle.

Acknowledgements

This work was supported by the National Natural Science Foundation of China (grant numbers 41875015, 42005069, and 42175180); the Special Fund (International Cooperation) Project for Science and Technology Innovation Strategy of Guangdong

Province (China, grant number 2019A050510021); Research and development projects in key areas of Guangdong Province (code 212020012620600004). The support from UK GCRF Rapid Response Grant on 'Transmission of SARS-CoV-2 virus in crowded indoor environment', the Opening Fund of State Key Laboratory of Green Building in Western China (No. LSKF202106), the Innovation Group Project of the Southern Marine Science and Engineering Guangdong Laboratory (Zhuhai) (No. 311020001), are also gratefully acknowledged. The supports by National Supercomputer Center in Guangzhou, P.R. China are also gratefully acknowledged.

References

[1] World Health Organization (WHO), Modes of transmission of virus causing COVID-19: implications for IPC precaution recommendations: scientific brief, (Accessed 29 March 2020). https://apps.who.int/iris/handle/10665/331616

[2] World Health Organization (WHO), WHO Coronavirus (Covid-19) Dashboard, (2021). https://covid19.who.int/

[3] S. Asadi, N. Bouvier, A. Wexler, W. Ristenpart, The coronavirus pandemic and aerosols: Does COVID-19 transmit via expiratory particles, Aerosol Sci. Technol. 54(6) (2020) 635-638. https://doi.org/10.1080/02786826.2020.1749229

[4] Y. Drossinos, N. Stilianakis, What aerosol physics tells us about airborne pathogen transmission, Aerosol Sci. Technol. 54(6) (2020) 639-643. https://doi.org/ 10.1080/ 02786826.2020.1751055

[5] J. Kutter, M. Spronken, P. Fraaij, R. Fouchier, S. Herfst, Transmission routes of respiratory viruses among humans, Curr. Opin. Virol. 28 (2018) 142-151. https://doi. org/10.1016/j.coviro.2018.01.001

[6] N. van Doremalen, T. Bushmaker, D. Morris, M. Holbrook, V. Munster, Aerosol and surface stability of SARS-CoV-2 as compared with SARS-CoV-1, N. Engl. J. Med. 382(16) (2020) 1564-1567. https://doi.org/10.1056/NEJMc2004973

[7] Y. Li, Basic routes of transmission of respiratory pathogens—A new proposal for transmission categorization based on respiratory spray, inhalation, and touch, Indoor Air 31(1) (2021) 3-6. https://doi.org/10.1111/ina.12786

669 [8] L. Marr, J. Tang, A Paradigm Shift to Align Transmission Routes With
670 Mechanisms, Clin. Infect. Dis. 73(10) (2021) 1747-1749. https://doi.org/10.1093/cid/
671 ciab722

672 [9] J. Hang, Y. Li, R. Jin, The influence of human walking on the flow and airborne
673 transmission in a six-bed isolation room: tracer gas simulation, Build. Environ. 77
674 (2014) 119-134. https://doi.org/10.1016/j.buildenv.2014.03.029

675 [10] Y. Li, H. Qian, J. Hang, X. Chen, P. Cheng, H. Ling, S. Wang, P. Liang, J. Li, S.
676 Xiao, Probable airborne transmission of SARS-CoV-2 in a poorly ventilated
677 restaurant, Build. Environ. 196 (2021) 107788. https://doi.org/10.1016/j.buildenv.
678 2021.107788

679 [11] C. Ou, S. Hu, K. Luo, H. Yang, J. Hang, P. Cheng, Z. Hai, S. Xiao, H. Qian, S.
680 Xiao, Insufficient ventilation led to a probable long-range airborne transmission of
681 SARS-CoV-2 on two buses, Build. Environ. 207 (2022) 108414. https://doi.org/10.
682 1016/j.buildenv.2021.108414

683 [12] M. Kang, J. Wei, J. Yuan, J. Guo, Y. Zhang, J. Hang, Y. Qu, H. Qian, Y.
684 Zhuang, X. Chen, Probable evidence of fecal aerosol transmission of SARS-CoV-2 in
685 a high-rise building, Ann. Intern. Med. 173(12) (2020) 974-980. https://doi.org/10.
686 7326/M20-0928

687 [13] X. Liu, J. Niu, K. Kwok, Analysis of concentration fluctuations in gas dispersion
688 around high-rise building for different incident wind directions, J. Hazard. Mater.
689 192(3) (2011) 1623-1632. https://doi.org/10.1016/j.jhazmat.2011.06.090

690 [14] X. Liu, J. Niu, K. Kwok, J. Wang, B. Li, Local characteristics of cross-unit
691 contamination around high-rise building due to wind effect: mean concentration and
692 infection risk assessment, J. Hazard. Mater. 192(1) (2011) 160-167. https://doi.org/10.
693 1016/j.jhazmat.2011.04.106

694 [15] Q. Wang, Y. Li, D. Lung, P. Chan, C. Dung, W. Jia, T. Miao, J. Huang, W.
695 Chen, Z. Wang, Aerosol transmission of SARS-CoV-2 due to the chimney effect in
696 two high-rise housing drainage stacks, J. Hazard. Mater. 421 (2022) 126799. https://
697 doi.org/10.1016/j.jhazmat.2021.126799

698 [16] I. Yu, Y. Li, T. Wong, W. Tam, A. Chan, J. Lee, D. Leung, T. Ho, Evidence of
699 airborne transmission of the severe acute respiratory syndrome virus, N. Engl. J. Med.
700 350(17) (2004) 1731-1739. https://doi.org/10.1056/nejmoa032867

701 [17] L. Liu, Y. Li, P. Nielsen, J. Wei, R. Jensen, Short-range airborne transmission of
702 expiratory droplets between two people, Indoor Air 27(2) (2017) 452-462. https://doi.
703 org/10.1111/ina.12314

[18] L. Liu, J. Wei, Y. Li, A. Ooi, Evaporation and dispersion of respiratory droplets from coughing, Indoor Air 27(1) (2017) 179-190. https://doi.org/10.1111/ina.12297

[19] F. Liu, Z. Luo, Y. Li, X. Zheng, C. Zhang, H. Qian, Revisiting physical distancing threshold in indoor environment using infection-risk-based modeling, Environ. Int. 153 (2021) 106542. https://doi.org/10.1016/j.envint.2021.106542

[20] N. Zhang, X. Chen, W. Jia, T. Jin, S. Xiao, W. Chen, J. Hang, C. Ou, H. Lei, H. Qian, B. Su, J. Li, D. Liu, Evidence for lack of transmission by close contact and surface touch in a restaurant outbreak of COVID-19, J. Infect. 83 (2021) 207-216. https://doi.org/ 10.1016/j.jinf.2021.05.030

[21] J. Hang, Y. Li, W. Ching, J. Wei, R. Jin, L. Liu, X. Xie, Potential airborne transmission between two isolation cubicles through a shared anteroom, Build. Environ. 89 (2015) 264-278. https://doi.org/10.1016/j.buildenv.2015.03.004

[22] H. Qian, Y. Li, P. Nielsen, C. Hyldgaard, T. Wong, A. Chwang, Dispersion of exhaled droplet nuclei in a two-bed hospital ward with three different ventilation systems, Indoor Air 16(2) (2006) 111-128. https://doi.org/10.1111/j.1600-0668. 2005.00407.x

[23] I. Bogoch, A. Watts, A. Thomas-Bachli, C. Huber, K. Khan, Pneumonia of unknown aetiology in Wuhan, China: potential for international spread via commercial air travel, J. Travel Med. 27(2) (2020) 1-3. https://doi.org/ 10.1093/ jtm/taaa008

[24] J. Gupta, C. Lin, Q. Chen, Transport of expiratory droplets in an aircraft cabin, Indoor Air 21(1) (2011) 3-11. https://doi.org/10.1111/j.1600-0668.2010.00676.x

[25] L. Oztig, O. Askin, Human mobility and coronavirus disease 2019 (COVID-19): a negative binomial regression analysis, Public Health 185 (2020) 364-367. https:// doi.org/10.1016/j.puhe.2020.07.002

[26] L. Zhang, Y. Li, Dispersion of coughed droplets in a fully-occupied high-speed rail cabin, Build. Environ. 47 (2012) 58-66. https://doi.org/10.1016/j.buildenv.2011. 03. 015

[27] S. Zhao, Z. Zhuang, J. Ran, J. Lin, G. Yang, L. Yang, D. He, The association between domestic train transportation and novel coronavirus (2019-nCoV) outbreak in China from 2019 to 2020: a data-driven correlational report, Travel Med. Infect. Dis. 33 (2020) 101568. https://doi.org/10.1016/j.tmaid.2020.101568

[28] X. Yang, C. Ou, H. Yang, L. Liu, T. Song, M. Kang, H. Lin, J. Hang, Transmission of pathogen-laden expiratory droplets in a coach bus, J. Hazard. Mater. 397 (2020) 122609. https://doi.org/10.1016/j.jhazmat.2020.122609

739 [29] R. Zheng, Y. Xu, W. Wang, G. Ning, Y. Bi, Spatial transmission of COVID-19
740 via public and private transportation in China, Travel Med. Infect. Dis. 34 (2020)
741 101626. https://doi.org/10.1016/j.tmaid.2020.101626

742 [30] C. Chao, P. Man, L. Morawska, G. Johnson, D. Katoshevski, Characterization of
743 expiration air jets and droplet size distributions immediately at the mouth opening, J.
744 Aerosol Sci. 40(2) (2009) 122-133. https://doi.org/10.1016/j.jaerosci.2008.10.003

745 [31] L. Morawska, G. Johnson, Z. Ristovski, M. Hargreaves, K. Mengersen, S.
746 Corbett, C. Chao, Y. Li, D. Katoshevski, Size distribution and sites of origin of
747 droplets expelled from the human respiratory tract during expiratory activities, J.
748 Aerosol Sci. 40(3) (2009) 256-269. https://doi.org/10.1016/j.jaerosci.2008.11.002

749 [32] J. Wei, Y. Li, Enhanced spread of expiratory droplets by turbulence in a cough
750 jet, Build. Environ. 93 (2015) 86-96. https://doi.org/10.1016/j.buildenv.2015.06.018

751 [33] X. Xie, Y. Li, A. Chwang, P. Ho, W. Seto, How far droplets can move in indoor
752 environments-revisiting the Wells evaporation-falling curve, Indoor Air 17(3) (2007)
753 211-225. https://doi.org/10.1111/j.1600-0668.2007.00469.x

754 [34] Y. Tung, Y. Shih, S. Hu, Numerical study on the dispersion of airborne
755 contaminants from an isolation room in the case of door opening, Appl. Therm. Eng.
756 29 (2009) 1544-1551. https://doi.org/10.1016/j.applthermaleng.2008.07.009

757 [35] J. Villafruela, I. Olmedo, J. José, Influence of human breathing modes on
758 airborne cross infection risk, Build. Environ. 106 (2016) 340-351. https://doi.org/10.
759 1016/ j.buildenv.2016.07.005

760 [36] Y. Yin, W. Xu, J. Gupta, A. Guity, P. Marmion, A. Manning, B. Gulick, X.
761 Zhang, Q. Chen, Experimental study on displacement and mixing ventilation systems
762 for a patient ward, HVAC R. Res. 15(6) (2009) 1175-1191. https://doi.org/10.1080/
763 10789669.2009.10390885

764 [37] R. Cermak, A. Melikov, Protection of occupants from exhaled infectious agents
765 and floor material emissions in rooms with personalized and underfloor ventilation,
766 HVAC R. Res. 13(1) (2007) 23-38. https://doi.org/10.1080/10789669.2007. 10390942

767 [38] J. Redrow, S. Mao, I. Celik, J. Posada, Z. Feng, Modeling the evaporation and
768 dispersion of airborne sputum droplets expelled from a human cough, Build. Environ.
769 46(10) (2011) 2042-2051. https://doi.org/10.1016/j.buildenv.2011. 04.011

770 [39] V. Yakhot, S. Orszag, Renormalization group analysis of turbulence. I. Basic
771 theory, J. Sci. Comput. 1(1) (1986) 3-51.

772 [40] T. Zhang, Q. Chen, Identification of contaminant sources in enclosed spaces by a
773 single sensor, Indoor Air 17(6) (2007) 439-449. https://doi.org/10.1111/j.1600-0668.
774 2007.00489.x

[41] Z. Zhang, W. Zhang, Z. Zhai, Q. Chen, Evaluation of various turbulence models in predicting airflow and turbulence in enclosed environments by CFD: Part 2—Comparison with experimental data from literature, HVAC R. Res. 13(6) (2007) 871-886. https://doi.org/10.1080/10789669.2007.10391460

[42] Z. Zhang, X. Chen, S. Mazumdar, T. Zhang, Q. Chen, Experimental and numerical investigation of airflow and contaminant transport in an airliner cabin mockup, Build. Environ. 44(1) (2009) 85-94. https://doi.org/10.1016/j.buildenv.2008.01.012

[43] Z. Zhang, Q. Chen, Comparison of the Eulerian and Lagrangian methods for predicting particle transport in enclosed spaces, Atmos. Environ. 41(25) (2007) 5236-5248. https://doi.org/10.1016/j.atmosenv.2006.05.086

[44] H. Qian, Y. Li, Removal of exhaled particles by ventilation and deposition in a multibed airborne infection isolation room, Indoor air 20(4) (2010) 284-297. https://doi.org/10.1111/j.1600-0668.2010.00653.x

[45] R. Clift, J. Grace, M. Weber, Bubbles, drops, and particles, Academic Press (1978). https://doi.org/10.1080/07373939308916817

[46] W. Hinds, Aerosol technology: properties, behavior, and measurement of airborne particles, John Wiley & Sons (1999).

[47] J. Potter, L. Matthews, J. Lemm, S. Spector, Human pulmonary secretions in health and disease, Ann. N. Y. Acad. Sci. 106(2) (1963) 692-697. https://doi.org/10.1111/j.1749-6632.1963.tb16677.x

[48] W. Ranz, Marshall, W., Evaporation from drops, Part II, Chem. Eng. Prog. 48(4) (1952) 7.

[49] P. Zhao, Y. Li, Correlation between the normal position of a particle on a rough surface and the van der Waals force, Colloids Surf. A Physicochem. Eng. Asp. 585 (2020) 124096. https://doi.org/10.1016/j.colsurfa.2019.124096

[50] A. Magar, M. Joshi, P. Rajagopal, A. Khan, M. Rao, B. Sapra, CFD simulation of the airborne transmission of covid-19 vectors emitted during respiratory mechanisms : Revisiting the concept of safe distance. ACS Omega 6 (2021) 16876–16889. https://doi.org/10.1021/acsomega.1c01489

[51] X. Shao, X. Li, COVID-19 transmission in the first presidential debate in 2020. Phys. Fluids 32 (2020) 1–9. https://doi.org/10.1063/5.0032847

[52] H. Qian, Y. Li, P. Nielsen, X. Huang, Spatial distribution of infection risk of SARS transmission in a hospital ward. Build. Environ. 44 (2009) 1651–1658. https://doi.org/10.1016/j.buildenv.2008.11.002

[53] G. Buonanno, L. Stabile, L. Morawska, Estimation of airborne viral emission: Quanta emission rate of SARS-CoV-2 for infection risk assessment. Environ. Int. 141 (2020) 105794. https://doi.org/10.1016/j.envint.2020.105794

[54]E. Riley, G. Murphy, R. Riley, Airborne spread of measles in a suburban elementary school, Am. J. Epidemiol. 107 (1978) 421-432. https://doi.org/10.1093/oxfordjournals.aje.a112560

[55] S. Zhang, Z. Lin, Dilution-based evaluation of airborne infection risk-Thorough expansion of Wells-Riley model, Build. Environ. 194 (2021) 107674. https://doi.org/10.1016/j.buildenv.2021.107674

[56] H. Dai, B. Zhao, Association of the infection probability of COVID-19 with ventilation rates in confined spaces, Build. Simul. 13 (2020) 1321-1327. https://doi.org/10.1007/s12273-020-0703-5

[57] H. Yang, T. Chen, Y. Lin, R. Buccolieri, M. Mattsson, M. Zhang, J. Hang, Q. Wang, Integrated impacts of tree planting and street aspect ratios on CO dispersion and personal exposure in full-scale street canyons. Build. Environ. 169 (2020) 106529. https://doi.org/10.1016/j.buildenv.2019.106529

[58] M. Mesgarpour, J. Abad, R. Alizadeh, S. Wongwises, M. Doranehgard, S. Ghaderi, N. Karimi, Prediction of the spread of Corona-virus carrying droplets in a bus-A computational based artificial intelligence approach, J. Hazard. Mater. 413 (2021) 125358. https://doi.org/10.1016/j.jhazmat.2021.125358

[59] W. Duan, D. Mei, J. Li, Z. Liu, M. Ja, S. Hou, Spatial distribution of exhalation droplets in the bus in different seasons, Aerosol Air Qual. Res. 21 (2021) 200478-200478. https://doi.org/10.4209/aaqr.200478

[60] S. Sun, J. Li, J. Han, How human thermal plume influences near-human transport of respiratory droplets and airborne particles: a review, Environ. Chem. Lett. 19 (2021) 1971-1982. https://doi.org/10.1007/s10311-020-01178-4

[61] C. Yang, X. Yang, B. Zhao, The ventilation needed to control thermal plume and particle dispersion from manikins in a unidirectional ventilated protective isolation room, Build. Simul. 8(5) (2015) 551-565. https://doi.org/10.1007/s12273-014-0227-6

[62] C. Chen, B. Zhao, Some questions on dispersion of human exhaled droplets in ventilation room: answers from numerical investigation, Indoor Air 20(2) (2010) 95-111. https://doi.org/10.1111/j.1600-0668.2009.00626.x

[63] A. Tsuda, F. Henry, J. Butler, Particle transport and deposition: basic physics of particle kinetics, Compr. Physiol. 3(4) (2013) 1437-1471. https://doi.org/10.1002/cphy.c100085

[64] W. Chen, N. Zhang, J. Wei, H. Yen, Y. Li, Short-range airborne route dominates exposure of respiratory infection during close contact, Build. Environ. 176 (2020) 106859. https://doi.org/10.1016/j.buildenv.2020.106859

[65] Y. Ji, H. Qian, J. Ye, X. Zheng, The impact of ambient humidity on the evaporation and dispersion of exhaled breathing droplets: A numerical investigation, J. Aerosol Sci. 115 (2018) 164-172. https://doi.org/10.1016/j.jaerosci.2017.10.009

[66] S. Zhu, S. Kato, J. Yang, Study on transport characteristics of saliva droplets produced by coughing in a calm indoor environment, Build. Environ. 41(12) (2006) 1691-1702. https://doi.org/10.1016/j.buildenv.2005.06.024

[67] Q. He, J. Niu, N. Gao, T. Zhu, J. Wu, CFD study of exhaled droplet transmission between occupants under different ventilation strategies in a typical office room, Build. Environ. 46(2) (2011) 397-408. https://doi.org/10.1016/j.buildenv.2010.08.003

[68] Z. Zhao, C. Xi, S. Mazumdar, T. Zhang, Q. Chen, Experimental and numerical investigation of airflow and contaminant transport in an airliner cabin mockup, Build. Environ. 44(1) (2009) 85-94. https://doi.org/10.1016/j.buildenv.2008.01.012

[69] A. Lai, W. Nazaroff, Modeling indoor particle deposition from turbulent flow onto smooth surfaces, J. Aerosol Sci. 31(4) (2000) 463-476. https://doi.org/10.1016/S0021-8502(99)00536-4

[70] W. Chen, H. Qian, N. Zhang, F. Liu, L. Liu, Y. Li, Extended short-range airborne transmission of respiratory infections, J. Hazard. Mater. 422 (2022) 126837. https://doi.org/10.1016/j.jhazmat.2021.126837

[71] M. Mirzaie, E. Lakzian, A. Khan, M. Warkiani, O. Mahian, G. Ahmadi, COVID-19 spread in a classroom equipped with partition–A CFD approach, J. Hazard. Mater. 420 (2021) 126587. https://doi.org/10.1016/j.jhazmat.2021.126587

[72] World Health Organization (WHO), Coronavirus disease (COVID-19): How is it transmitted, (Accessed 13 December 2020). https://www.who.int/news-room/q-a-detail/coronavirus-disease-covid-19-how-is-it-transmitted

[73] American Society of Heating, Refrigerating and Air-Conditioning Engineers (ASHRAE) Ventilation for acceptable indoor air quality, ASHRAE Standard, Atlanta, USA (2019).

[74] D. Etheridge, M. Sandberg, Building ventilation: theory and measurement, John Wiley & Sons Chichester, UK (1996).

[75] P. Cheng, K. Luo, S. Xiao, H. Yang, J. Hang, C. Ou, B. Cowling, H. Yen, D. Sc, S. Hu, Y. Li, Predominant airborne transmission and insignificant fomite transmission of SARS-CoV-2 in a two-bus COVID-19 outbreak originating from the same pre-symptomatic index case. J. Hazard. Mater. 425 (2022) 128051. https://doi.org/10.1016/ j.jhazmat.2021.128051

882 [76] J. Gupta, C. Lin, Q. Chen, Inhalation of expiratory droplets in aircraft cabins,
883 Indoor Air 21(4) (2011) 341-350. https://doi.org/10.1111/j.1600-0668.2011.00709.x
884
885